STANFORD
UNIVERSITY

Final Report
NASA NIAC Phase I Study

Spacecraft/Rover Hybrids for the Exploration of Small Solar System Bodies

Prepared for
Dr. John M. Falker
Program Executive, NASA Innovative Advanced Concepts Program

Submitted September 30, 2012

Submitted by
Prof. Marco Pavone, PI
Department of Aeronautics and Astronautics
Stanford University
496 Lomita Mall, Room 261, Stanford, CA 94305-4035
Phone: (650)723 4432
Email: pavone@stanford.edu

Dr. Julie C. Castillo-Rogez, Co-I
Jet Propulsion Laboratory
California Institute of Technology
Email: julie.c.castillo@jpl.nasa.gov

Prof. Jeffrey A. Hoffman, Co-I
Massachusetts Institute of Technology
Department of Aeronautics and Astronautics
Email:jhoffma1@mit.edu

Dr. Issa A. D. Nesnas, Co-I
Jet Propulsion Laboratory
California Institute of Technology
Email: issa.a.nesnas@jpl.nasa.gov

Executive Summary

This study investigated a novel mission architecture for the systematic and affordable *in-situ* exploration of small Solar System bodies. Specifically, a mother spacecraft would deploy over the surface of a small body one, or several, spacecraft/rover hybrids, which are small, multi-faceted enclosed robots with internal actuation and external spikes. They would be capable of 1) long excursions (by hopping), 2) short traverses to specific locations (through a sequence of controlled tumbles), and 3) high-altitude, attitude-controlled ballistic flight (akin to spacecraft flight). Their control would rely on synergistic operations with the mother spacecraft (where most of hybrids' perception and localization functionalities would be hosted), which would make the platforms minimalistic and, in turn, the entire mission architecture affordable, see Figure 1.

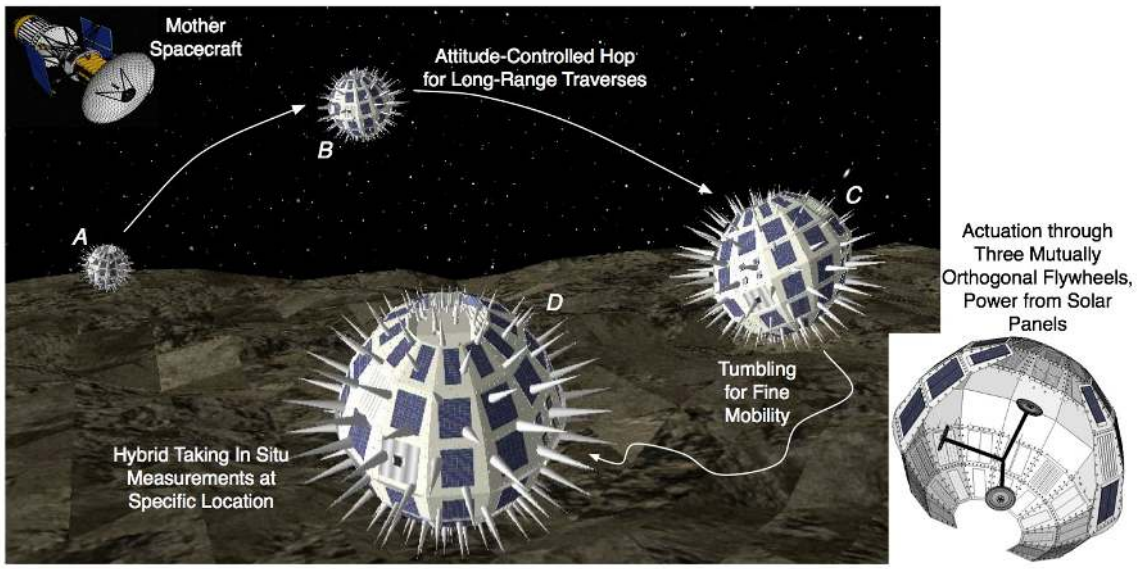

Figure 1: The mission architecture: one mother spacecraft would deploy on the surface of a small body one (or more) spacecraft/rover hybrids (from cm- to m-scale). Once deployed, the hybrids would perform attitude-controlled hops for long-range traverses (on the order of 10 m per hop, steps A to B to C in the figure) and would tumble to reach specific locations (steps C to D in the figure). Each hybrid is sealed in one enclosure and internally actuated through three mutually orthogonal flywheels (see bottom-right figure). Synergistic mission operations would ensure precise planning and control of the hybrids, while keeping their end-to-end design minimalistic.

The Phase I study was aimed at providing an initial feasibility assessment of the proposed architecture and had, in particular, four main objectives: 1) to characterize the expected science return of spatially-extended in-situ exploration at small Solar System bodies, 2) to demonstrate that a hybrid can achieve both large surface coverage via hopping and fine mobility via tumbling in low gravity environments (specifically, for a boulder-free environment with a gravity level on the order of mm/s^2, the requirement was 20%-30% motion accuracy with an average speed on the order of cm/s); 3) to provide first-order estimates for the critical subsystems, and 4) to study mission operations and a mission scenario to Phobos.

The main results of our study can be summarized as follows:

- **Science rationale**: We investigated the expected science return of spatially extended

in-situ exploration at small Solar System bodies in the context of the key science priorities identified by the decadal survey report *Vision and Voyages* [1]. Targets within the scope of our analysis belonged to three main classes: main belt asteroids and irregular satellites, Near Earth Objects, and comets. For each class of targets, we linked science objectives with required measurements, instruments, and mission architectures. The conclusion of our analysis is that spatially-extended in-situ information about the chemical and physical heterogeneity of small bodies has the potential to lead to a much improved understanding about the origin, evolution, and potential astrobiology of such objects, and, in general, of the Solar System. This is essentially due to the variety in surface properties at scales as low as few meters, as determined for a number of potential exploration targets (with a special focus on Mars' moon Phobos).

- **Hybrids' dynamics and control**: We developed analytical and numerical models for the hybrids, we characterized their dynamics (including fundamental limitations of performance) and we developed control and planning algorithms. Preliminary results within a simulated environment showed that, on smooth terrains with gravity levels on the order of $\mathrm{mm/s^2}$, a hybrid can achieve motion accuracy on the order of 10% over distances of dozens of meters with velocities on the order of several cm/s (see Figure 2). This result increases our confidence in the ability to control the motion of the hybrids to reach designated targets. It also fulfills the requirements set forth in the Phase I study about mobility control in a benign environment. We used simulation results to develop two prototypes, which were validated on two microgravity test stands (developed ad hoc for this project), see Figures 3 and 4. Experimental results showed a strong correlation among the results from the micro-gravity test stands, the analytical models, and the numerical simulations. Further simulations over rough terrains and higher fidelity models for the hybrid/terrain interaction are necessary to demonstrate hybrids' fine mobility on harsh planetary surfaces, but our current results are promising.
- **Hybrid's feasibility**: We computed first-order estimates of critical subsystems such as power, thermal, and communication. We calculated power, thermal, and mass budgets for a hybrid exploring the Stickney crater on Phobos. We determined that most subsystems could be implemented with existing technologies. One important exception is the power subsystem, which would require further study to extend hybrids' lifetime beyond the current two-day limit.
- **Mission operations**: We performed a preliminary study for mission operations, under the assumption that the mothership is already in proximity of the target body. We determined that proximity operations should include four phases, namely "initial reconnaissance of target", "deployment", "hybrid's initial free roaming", and "command and execute guided trajectories". In particular, we studied both in-situ deployments and deployments from a distance, and for a reference mission to Phobos we determined that 3 m/s is approximately the touchdown speed from the Halo orbit at Mars-Phobos L1 (while this may seem fast, note that is the equivalent of dropping an object from a height of ≈ 50 cm on the Earth). After a trade-off analysis, we determined that, to keep the design of a hybrid as minimalistic as possible, the hybrid should rely on *synergistic mission operations*, wherein the mothership bears the primary responsibility for determining the position and orientation of the hybrid, and the mobile platform is only responsible for local perception.

- **Reference mission to Phobos**: We developed a high-level mission study for a reference mission to Phobos. We characterized a science traceability matrix and we assessed that the required motion accuracy, given the scale of the landmarks to be visited, should be on the order of $20\% - 30\%$; this requirement compares well with the capabilities of a hybrid. We determined a "minimalistic" baseline design for the hybrid; its total mass would be about 5 kg, its size about $0.5\,\mathrm{m}^3$, and the average power requirement would be approximately 15 Watts. In our mission concept, a single-string electric propulsion mothership would deploy from a distance one, or more, hybrids on the surface of Phobos in proximity of the Stickney crater. The hybrids would carry a X-ray spectrometer, a radiation monitor, a thermocouple, and a microscope, and would operate for about 48 hours over a surface of about $1 - 5\,\mathrm{Km}^2$. The mothership would be equipped with a gamma ray and neutron detector, a high-resolution stereo camera, a radio science subsystem, and a dust analyzer, and would station keep at the Mars-Phobos L1 point. Using orbital observations, mission planners would upload traverse sequences to the hybrids via the mothership (see Figure 5). Major science objectives would be to characterize regolith composition, evaluate regolith maturity, constrain mechanical properties, constrain dust dynamics, achieve both topography and gravity mapping, study surface dynamics and the electrostatic environment, and characterize the distribution of water. Note that these objectives can only be achieved by complementing the measurements taken by the mothership with those taken in-situ by the hybrids.

In summary, in the Phase I study we demonstrated that the bounding assumptions behind our proposed mission architecture are reasonable, with a sound scientific and engineering basis. A future study should focus on the key feasibility and maturation aspects identified during Phase I, in particular, hybrids' fine mobility on irregular terrains, life-expanding power subsystems, and synergistic mission operations.

This study led to four publications:

- M. Pavone, J. C. Castillo-Rogez, J. A. Hoffman, I. A. D. Nesnas, "Spacecraft/Rover Hybrids for the Exploration of Small Solar System Bodies," 2013 IEEE Aerospace Conference (submitted, abstract approved).

- R. Allen, M. Pavone, C. McQuin, I. A. D. Nesnas, J. C. Castillo-Rogez, T.-N. Nguyen, J. A. Hoffman, "Internally-Actuated Rovers for All-Access Surface Mobility: Theory and Experimentation," in 2013 IEEE Int. Conf. on Robotics and Automation (submitted).

- M. Pavone, J. Castillo-Rogez, J. A. Hoffman, I. A. D. Nesnas, N. J. Strange, "Optimizing Decadal and Precursor Science on Small Solar System Bodies with Spacecraft/Rover Hybrids," in 2012 American Geophysical Union Fall Meeting.

- J. Castillo-Rogez, M. Pavone, I. A. D. Nesnas, J. A. Hoffman, "Expected Science Return of Spatially-Extended In-Situ Exploration at Small Solar System Bodies," in 2012 IEEE Aerospace Conference.

Technical papers, related presentations, movies of the experiments, etc. can be found at the project's website: `http://www.stanford.edu/~pavone/niac.html`.

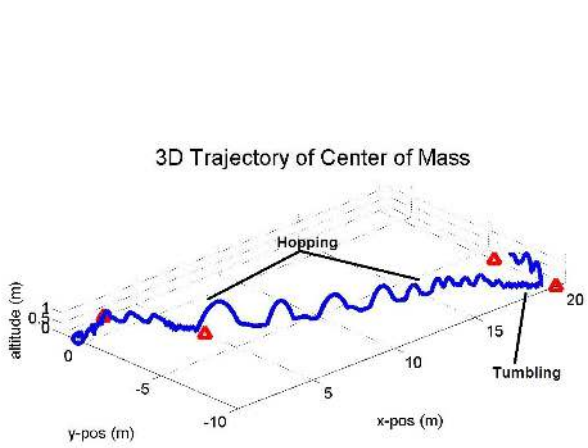

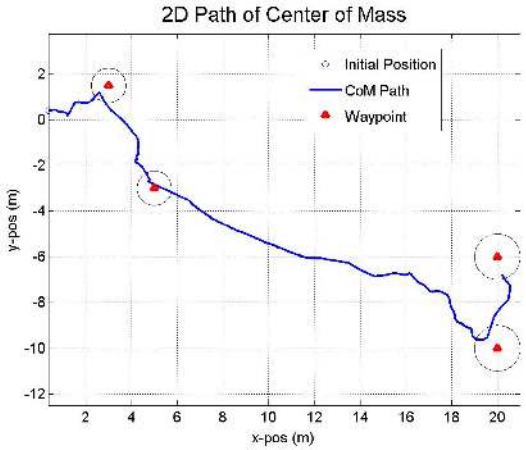

Figure 2: Demonstration of *controlled* mobility (as opposed to random hopping motion): the plots represent the application of motion planning and control algorithms under Phobos-like conditions (i.e., gravity levels on the order of $\mathrm{mm/s^2}$). Waypoints were selected to demonstrate short and long traverses and directional changes. The hybrid averages a velocity of $\approx 1.6\,\mathrm{cm/s}$ over the 1770 seconds it takes to visit the four waypoints. The motion accuracy is on the order of 10%; the simulation results assume a smooth surface.

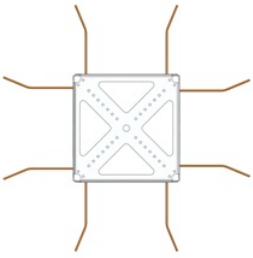

Figure 3: Prototype and CAD models (not to scale). The prototype, without the flywheel, has a mass of 1.39 kg and a moment of inertia about the axis of rotation of $\approx 0.054\,\mathrm{kg\,m^2}$. The flywheel is 0.57 kg and $8.07 \times 10^{-4}\,\mathrm{kg\,m^2}$.

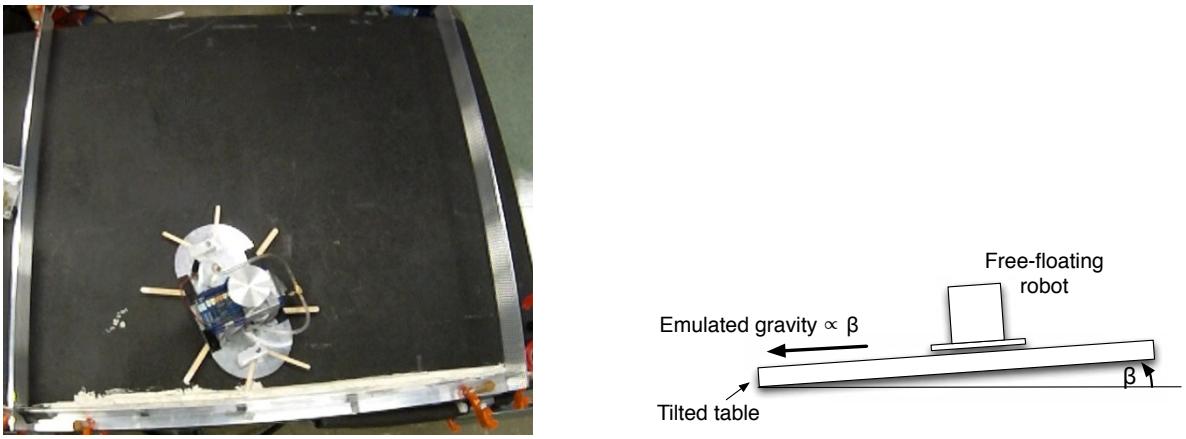

Figure 4: 3 DOF test stand on a frictionless table; by tilting the granite table, one can create a "small" force that emulates a low gravity field.

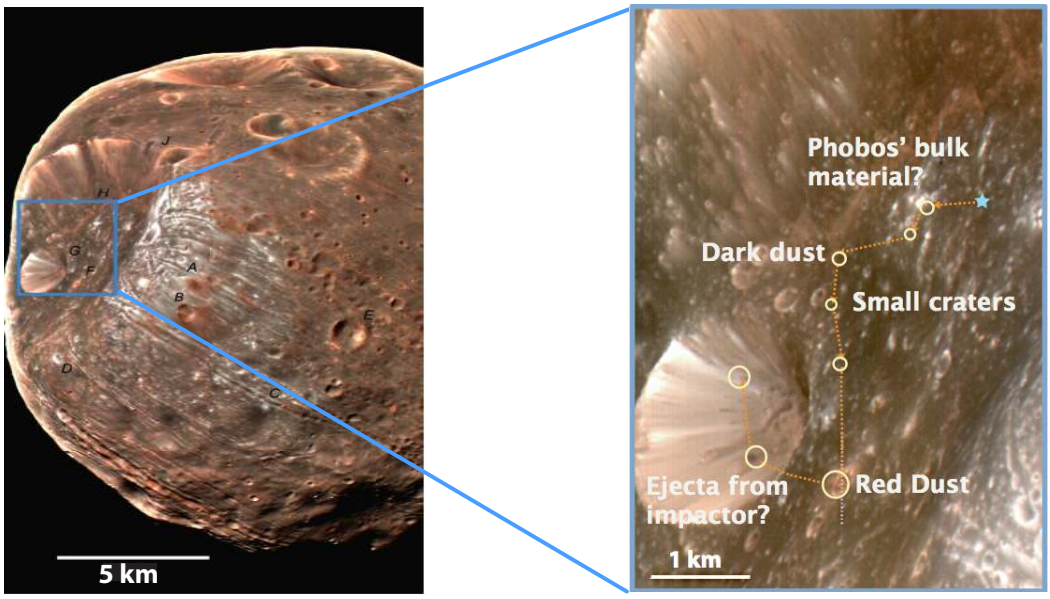

Figure 5: Notional illustration of the trajectory that a hybrid should execute in order to sample both the chemical and the physical diversity on Phobos (close to the Stickney crater). The motion accuracy, given the scale of the landmarks to be visited, should be on the order of $20\% - 30\%$, which compares well with the capabilities of a hybrid.

Contents

1 Introduction

The recent decadal survey report for planetary science has prioritized three main cross-cutting themes for planetary exploration: (1) the characterization of the early Solar System history, (2) the search for planetary habitats, and (3) an improved understanding about the nature of planetary processes [1]. A growing number of ground and space observations indicate that the exploration of a selected subset of small Solar System bodies would collectively address all of such themes. The exploration of small bodies such as Near Earth Objects and Mars' moons is also a key component of the flexible path for human exploration. In general, origins science and the search for habitats revolve around characterizing planetary material chemistry (elemental, isotopic, mineralogical, noble gas, organics, etc.). While some measurements can be obtained with remote platforms (such as space telescopes or orbiting spacecraft), several other measurements require direct contact with (or close proximity to) the surface for an *extended* period of time at *multiple* locations. This is also the case for precursor science enabling human exploration, which requires the characterization of regolith mechanical properties, dust dynamics, electrostatic charging, etc. [2]. Hence, in-situ exploration of small bodies at multiple designated locations is an important need in the scientific community and requires surface mobility.

Current mission architectures for the in-situ, multi-point exploration of small Solar System bodies tend to be high-cost and/or unable to ensure targeted sampling. On the one hand, monolithic architectures, which entail landing a spacecraft multiple times (as in the Comet Hopper mission architecture, pre-selected by NASA for a Discovery-class mission [3]), only allow for limited *discrete* and *random* sampling (versus spatially dense and targeted sampling, which requires surface mobility and is key for understanding, e.g., the nature of the interface between two spectral units), might lead to surface contamination (due to firing thrusters), and might involve high risks during each surface sortie, which translate into high-cost risk mitigation strategies. On the other hand, multi-asset architectures, which entail the deployment of mobile platforms, have to *overcome* the lack of gravity. Specifically, in low gravity environments wheeled vehicles are bound to extremely low speeds (less than 1.5mm/s [4]) due to low traction, and surface bumps can cause loss of surface contact and uncontrolled tumbling. Alternatively, legged systems are mechanically complex and highly dependent on soil properties [5, 6], which are largely unknown. NASA, RKA, ESA, and JAXA have all recognized the advantages of hopping on small bodies. However, both of NASA's hopper prototypes [4, 7] (that rely on a combination of wheels and sticking mechanisms), ESA's hopper prototype (that hops by spinning two eccentric masses [8]), RKA's landers for the failed exploration of Phobos (that hop by sticking the surface [9]), and JAXA's MINERVA lander (that hops by rotating a single flywheel mounted on a turntable and did not succeed during its deployment [10]) do not allow for precise traverses to designated targets. Furthermore, their surface operations (in terms of perception and planning) are essentially independent of the mothership (used as a communication "bent pipe"), which makes such platforms fully-fledged spacecraft in their own right.

This report describes a novel mission architecture for the systematic and affordable in-situ exploration of small Solar System bodies. Specifically, a mother spacecraft would deploy over the surface of a small body one, or several, spacecraft/rover hybrids, which are small, multi-faceted enclosed robots with internal actuation (critically *enabled* by microgravity)

and external spikes. They would be capable of 1) long excursions (by hopping), 2) short traverses to *specific* locations (through a sequence of controlled tumbles), and 3) high-altitude, attitude-controlled ballistic flight (akin to spacecraft flight). Their control would rely on *synergistic operations* with the mother spacecraft (where most of hybrids' perception and localization functionalities would be hosted), which would make the platforms *minimalistic* and, in turn, the entire mission architecture affordable, see Figure 6.

This report is structured as follows. In Section 2 we summarize our study about the expected science return of spatially-extended in-situ exploration at small bodies. In Section 3 we characterize the dynamics of the hybrids (including fundamental limitations of performance), we discuss control and planning algorithms, we discuss the development of a prototype, and we present experimental results both in simulations and on physical test stands emulating low-gravity environments. In Section 4 we provide first order estimates of critical subsystems such as power, communication, thermal, etc. In Section 5 we discuss a four-phase mission operation concept and we present a traceability matrix and a preliminary mission analysis for a Phobos mission scenario. Finally, in Section 6, we draw our conclusions.

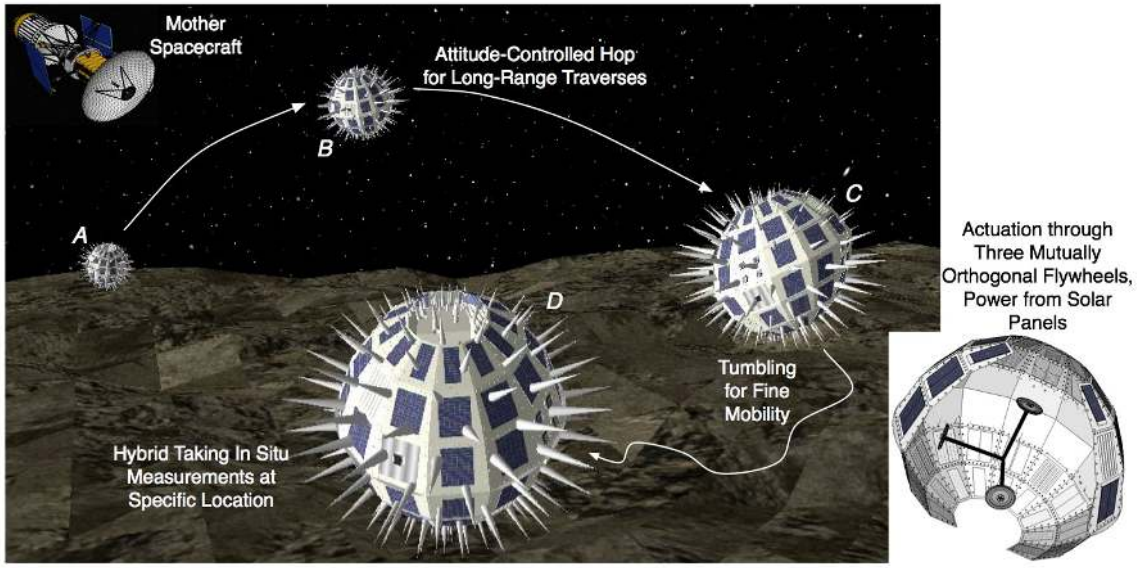

Figure 6: The mission architecture: one mother spacecraft would deploy on the surface of a small body one (or more) spacecraft/rover hybrids (from cm- to m-scale). Once deployed, the hybrids would perform attitude-controlled hops for long-range traverses (on the order of 10 m per hop, steps A to B to C in the figure) and would tumble to reach specific locations (steps C to D in the figure). Each hybrid is sealed in one enclosure and internally actuated through three mutually orthogonal flywheels (see bottom-right figure). Synergistic mission operations would ensure precise planning and control of the hybrids, while keeping their end-to-end design minimalistic.

2 Business case and science focus

In Phase I we have performed a comprehensive study of the expected science return of small bodies exploration, with a focus on spatially-extended in-situ observations[1]. In summary, data obtained from recent missions show that surface properties on most small bodies evolve over scales of hundreds of meters to as little as *few meters* (Figure 7 highlights the diversity in surface properties at a variety of scales for a number of representative objects); this is in contrast to the long-held idea that small bodies' surfaces are, in general, both chemically and physically homogenous. As a consequence, surface mobility is *pivotal* to properly constrain soil properties and surface physics, provided that science instruments can be fitted within the mobile platforms. A review of the literature revealed that many miniaturized (< 1 kg) instruments have been flown and already achieved TRL 6 and higher (e.g., tunable laser spectrometer; heat flow probe on Deep Space 2; X-ray spectroscopy on Beagle 2; cameras on multiple missions). Analytical measurement techniques (essential for origins science) have lower TRL but are the focus of current investment by NASA, in its instrument definition programs.

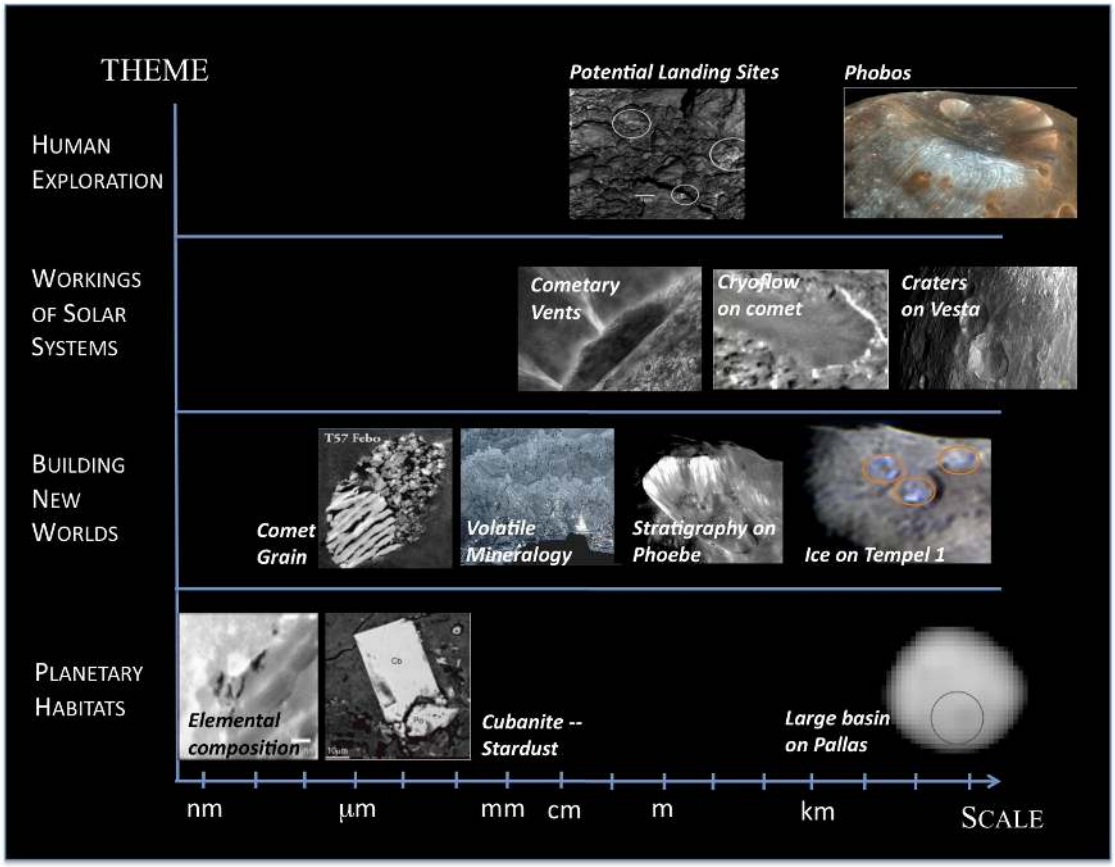

Figure 7: Illustration of the type of observations needed in order to successfully address the key science pertaining to the three cross-cutting themes highlighted in *Vision and Voyages*. Note that in general we lack high-resolution observations at the mm to the meter scale that could be best obtained by in-situ exploration.

[1]This section presents a summary of our findings; all the details can be found in our paper [11].

In this section we first show that the exploration of a selected subset of small bodies would collectively address the key science priorities identified by the survey report *Vision and Voyages* for planetary science (compiled by the National Research Council (NRC), [1]); then, we focus on three classes of small bodies (asteroids and irregular satellites, comets, and near-Earth objects (NEOs)) for which spaceborne observations are available. For each class of targets, we identify the science objectives for their exploration, we discuss the types of measurements, instruments, and mission architectures that would be required, and we discuss the importance of spatially-extended in-situ observations to fulfill the scientific goals.

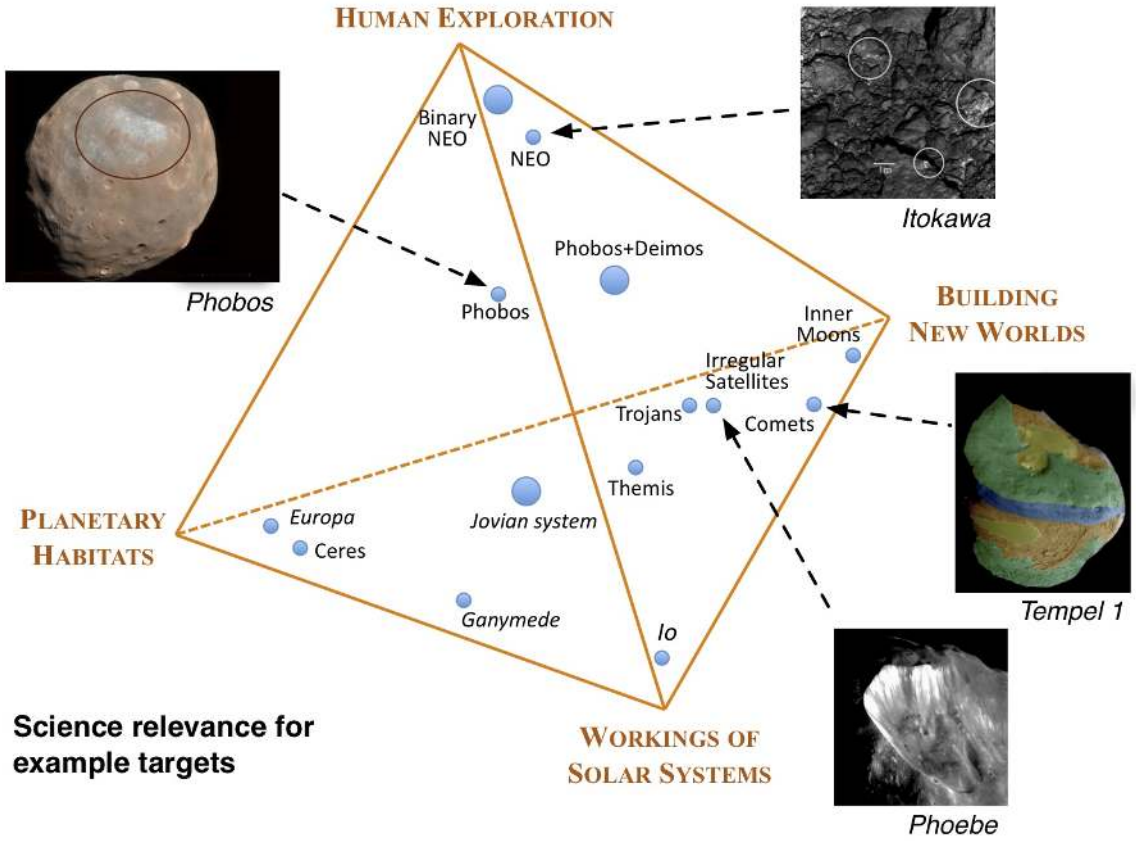

Figure 8: Relevance of different small bodies with respect to the three themes of the decadal survey report and to the vision for future human exploration (represented as corners of the polygon). The position of a target within the polygon represents its relative relevance with respect to the science themes and to the human exploration vision. For example, comets are expected to be among the most primitive objects in the Solar System although space observations indicate that they also exhibit a large variety of landscapes that result from long-term geological activity (hence their position is in between two corners of the polygon). Another example is Phobos whose surface exploration would pertain to all four themes, as detailed in this report. The exploration of several components of a multinary system is expected to increase the overall science return of a mission, which is symbolized by bigger circles.

2.1 Science objectives of small bodies exploration

In March 2011 the National Research Council has released the planetary science decadal survey 2013-2022 *Vision and Voyages* [1]. The NRC committee has organized the basic

motivations for next-decade planetary research into three cross-cutting themes:

Building New Worlds theme: i.e., understanding Solar System beginnings.
Planetary Habitats theme: i.e., searching for the requirements for life.
Workings of Solar Systems theme: i.e., revealing planetary processes through time.

In the following, we discuss how the exploration of a subset of small bodies would collectively contribute to all of the three cross-cutting themes, and we also discuss their relevance in the context of future Human Exploration programs. Our findings are summarized in Figure 8 and Table 1 (that includes information about key observations, instruments, and targets).

2.1.1 Small bodies and "Building New Worlds" theme

Most small bodies, being building blocks of the Solar System, are of pivotal importance within the "Building New World" theme. The current state of the art (known as "Nice" model) is that resonances between Jupiter and Saturn led to the redistribution of planetesimals throughout the Solar System during its first million years (My), and then later during the "late cataclysm" (also know as "late heavy bombardment") about 700-800 My ago [12], [13], [14]. Key aspects of the model that may be testable are that (a) all asteroids in Jupiter's Lagrangian points come from the outer Solar System [14]; (b) wet asteroids throughout the main belt and Hilda group of asteroids share a genetic link with Jupiter's Trojan asteroids and outer planet irregular satellites [15]; (c) most of the volatiles accreted in the Solar System were supplied by outer Solar System planetesimals [16]. Therefore, small bodies play a central role in the validation (or confutation) of the Nice model, and more in general for understanding the origin of volatiles and organics on Earth (and on Mars).

2.1.2 Small bodies and "Planetary Habitats" theme

A variety of recent observations have shed new light on the astrobiological relevance of small bodies. For example, ground-based observations have led to the identification of water ice at the surface of large main belt asteroids 24 Themis [17, 18] and 65 Cybele [19]. The detection of crystalline ice and ammonia hydrates at Charon [20] and of carbonates at the surface of Ceres [21] suggest that these two dwarf planets present recent or ongoing endogenic activity [22, 23]. Albedo variations at the surface of Pallas [24] indicate that this large asteroid is differentiated and the regions excavated by impacts are rich in organics [23].

2.1.3 Small bodies and "Workings of Solar Systems" theme

The relevance of small bodies to this theme is multifold, since they are subject to a variety of processes (some of them unique, e.g., cryovolcanism). Many of these processes tend to smooth out the surface; examples include a) flow of regolith and dust material along cliffs and in consequence to seismic activity, b) chemical weathering (that causes the darkening of surface material), and c) weathering due to solar wind (that happens on a scale of just a few My) [25]. Another important process is cometary outgassing, whose driving mechanism has not been fully elucidated. This process depends in part on the nature of volatiles present on comets, and in particular on the way such volatiles are trapped: either encaged in clathrate hydrates or adsorbed in amorphous ice.

2.1.4 Small bodies and Human exploration

Small bodies (especially NEOs) are also central to the President's Vision of sending humans to Mars within the next decades. In fact, given their vicinity (for NEOs) and low gravity, they represent ideal targets for precursor missions. Besides NEOs, Mars' moons Phobos and Deimos are also envisioned as key targets for human exploration (see Table 1).

2.2 In-situ sampling driving science return

Tables 2, 3, and 4 link science objectives with required measurements, instruments, and mission architectures for, respectively, asteroids, comets, and NEOs; one can observe how spatially-extended in-situ observations are needed to fulfill the majority of science objectives. This is essentially due to the variety in surface properties at scales as low as few meters (see also Figure 7). The scientific need for in-situ observations at multiple designated locations and within a short distance is corroborated by the following examples.

Multiple location sampling Consider comet Tempel 1. Such comet presents four distinct geological units; in particular, it exhibits cryoflow features (that are products of geological evolution) near areas that appear to be less evolved and may be more representative of the original material. Hence, a spatially-extended exploration of Tempel 1 would be pivotal to capture information on the accretional environment of that object as well as on its long-term evolution. Additionally, spatially-extended coverage may also imply sampling the various components of a planetary system, for example, the two components of a binary asteroid system, or a subset of asteroids within the main belt (to probe the chemical gradient, which plays a special role in the Nice model [26]), or several NEOs during the course of one mission in order to evaluate the diversity of physical properties. In situ exploration of Phobos would most probably solve the mystery of the origin of that satellite. However, the combined exploration of both Phobos and Deimos would lead to a far more fundamental understanding of the early history of the Martian system, the origin of Mars' volatiles, and the genetic relationship between Mars and Earth. In-situ observations at multiple locations could also help assess the risk posed by certain environmental conditions, such as electric charging and dust levitation, as a first step toward human missions.

Sampling designated locations The exploration of specific, short-scale features (which would require fine mobility) appears to be of primary importance for small body exploration. An example is represented by designated, small-scale features in proximity of craters. Craters are generally interesting locations to study because they present excavated material, which can represent either the bulk of the object near to a lag deposit or regoliths resulting from space weathering [27]. Other small-scale features of scientific importance are represented by ice-rich and/or organic-rich features (Fig. 10c), outstanding features such as ejecta, boulders, tectonic faults (e.g., Enceladus' Tiger stripes). Targeted, in-situ *reconnaissance* would also be an important component of potential future sample return missions, such as the *Comet Surface Sample Return*, by sending one or multiple mobility platforms to identify compelling sample sites of the surface prior to sampling.

2.3 Summary

In summary, our work highlights the scientific importance of small bodies' exploration and of mission architectures for their study that involve in-situ measurements at multiple designated locations. This is essentially due to the variety in surface properties at scales as

Themes	Key Science Priorities	Key Observations	Key Instruments	Key Targets
Building new worlds	What were the initial stages, conditions and processes of Solar System formation and the nature of the interstellar matter that was incorporated?	Elemental, mineralogical, isotopic composition	NIR, mid-IR, TIR, UV, GR&ND, MS, XRD/XRF; Sample Return	Comets, NEOs, Phobos, Deimos, main belt and Trojan asteroids, irregular satellites
	How did the giant planets and their satellite systems accrete, and is there evidence that they migrated to new orbital positions?	Isotopic composition, dynamical properties	MS, high-resolution imaging; Sample Return	Irregular satellites, inner planetesimal satellites
	What governed the accretion, supply of water, chemistry, and internal differentiation of the inner planets and the evolution of their atmospheres, and what roles did bombardment by large projectiles play?	Isotopic composition, nature and abundance of volatiles (elemental and mineralogical composition), venting	MS, mid-IR, NIR, UV, GPR; Sample Return	NEOs, C- and D-asteroids, comets
Planetary habitats	What were the primordial sources of organic matter, and where does organic synthesis continue today?	Search for organics, signature of hydrothermal environment	mid-IR, NIR, XRF, APXS; Sample Return	C-asteroids, Trojan asteroids, NEOs, comets
	Beyond Earth, are there contemporary habitats elsewhere in the Solar System with necessary conditions, organic matter, water, energy, and nutrients to sustain life, and do organisms live there now?	Organics, temperature, water bio-signatures, endogenic and geological activity, presence of a deep ocean, surface environments, (temperature, radiations, etc.)	Thermal mapper, GPR, gravity, mid-IR, RPWS, High-res imaging	Icy satellites, TNOs, comets, large wet asteroids, Phobos
Workings of Solar Systems	How do the giant planets serve as laboratories to understand Earth, the Solar System, and extrasolar planetary systems?	Collision processes, dust distribution	High-res imaging, Dust Analyzer	Satellites (inner, medium/large, irregular)
	What Solar System bodies endanger and what mechanisms shield Earth's biosphere?	Population survey, dynamical properties characterization	Mid-IR, TIR, NIR, UV, High-res imaging	NEOs, comets
	Can understanding the roles of physics, chemistry, geology, and dynamics in driving planetary atmospheres and climates lead to a better understanding of climate change on Earth?	Surface morphology, search for cryovolcanic activity	High-res imaging, Thermal Mapper	Comets, Enceladus
	How have the myriad chemical and physical processes that shaped the Solar System operated, interacted, and evolved over time?	Regolith properties, global physical structure, surface chemistry	Gravity, GPR, High-res imaging, RPWS	Any object
Human exploration	Risk reconnaissance	Surface morphology at all scales, dynamical properties, mechanical properties, electrostatic charging, dust dynamics	Dust analyzer, High-res imaging, rover motion	NEOs, Phobos, Deimos
	In situ resource utilization	Search for water abundance and distribution, physical structure	GPR, GR&ND, gravity; Sample Return	NEOs, Phobos, Deimos
	Reconnaissance of scientific significance	Heat flow and thermal structure, deep interior properties, dynamics		NEOs, Phobos, Deimos

Table 1: Traceability matrix for the key science priorities highlighted in the decadal survey report, with a focus on small bodies exploration. Acronyms used: APXS := Alpha-Particle-X-Ray; GPR := Ground-Penetrating Radar; GR := Gamma Ray; MS := Mass Spectrometry; ND := Neutron Detection; NIR := Near Infra-Red; RPWS := Radio and Plasma Wave Science; TIR := Thermal Infra-Red spectroscopy; UV := Ultra-Violet Spectroscopy; XRD := X-Ray Diffraction; XRF := X-Ray Fluorescence; High-Res := High-Resolution. Note that many miniaturized (< 1 kg) instruments have been flown and already achieved TRL 6 and higher (e.g., tunable laser spectrometer, heat flow probe, X-ray spectroscopy, cameras, etc.). However, analytical measurement techniques (essential for origins science) have lower TRL but are the focus of current investment by NASA, in its instrument definition programs.

low as few meters (see Figure 7). As shown in Tables 1, 2, 3, and 4, in-situ exploration would involve a combination of non-analytical and analytical instruments, which should be miniaturized if embedded in a small-scale surface mobility platform; while miniaturized non-analytical instruments have been flown and already achieved TRL 6, their analytical counterparts present a lower TRL and represent a feasibility issue. In this section we have not quantitatively discussed the mobility accuracy that a surface mobility platform should achieve; this heavily depends on the target body, and has been studied in some detail within a reference mission to Phobos, see Section 5.

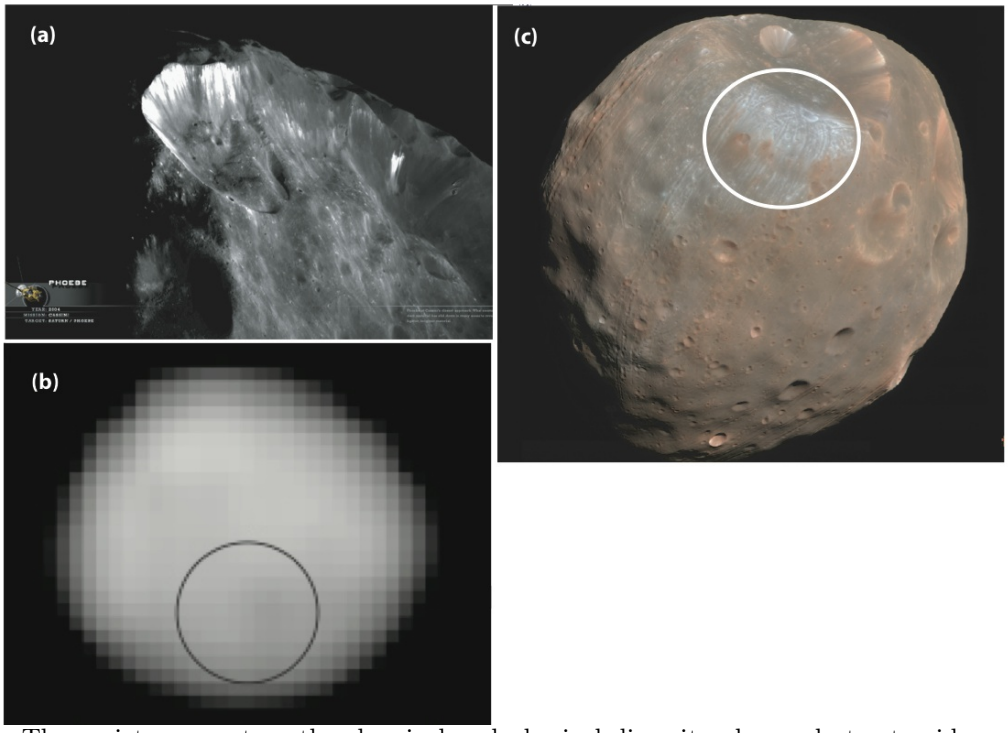

Figure 9: These pictures capture the chemical and physical diversity observed at asteroids and irregular satellites. (a) North pole of Saturn's satellite Phoebe obtained by the Cassini-Huygens mission; while the satellite's albedo is less than 0.1, high-albedo material can be seen on crater walls, which suggests that the dust cover is only a few tens of meter thick (Credit: NASA/ISS/CICLOPS). (b) Pallas' surface as seen by the Hubble Space telescope [24]; the circle indicates a low-albedo area associated with a large impact basin. (c) Phobos by HiRISE on the Mars Reconnaissance Orbiter; lateral variations in color properties suggest that Phobos' material has different origins (Credit: NASA/University of Arizona).

Objectives	Observations	Measurements	Architecture
Constrain accretional environment	Density, volatile composition, isotopic ratios	Radio science, NIR, mid-IR, TIR, MS, TLS/LIBS, Raman	Orbiter, in-situ
Constrain dynamical evolution	Orbital properties, cratering properties, rotational properties	High resolution imaging (WAC+NAC), gravity	Orbiter, surface beacon
Characterize surface environment	Fields and waves	MAG, RPWS	Orbiter
Evaluate astrobiological potential	Geological activity, biomakers, outgassing, magnetic field	High-resolution imaging, NIR, mid-IR, UV, MS, MAG	Orbiter, in-situ

Table 2: Asteroids and irregular satellites.

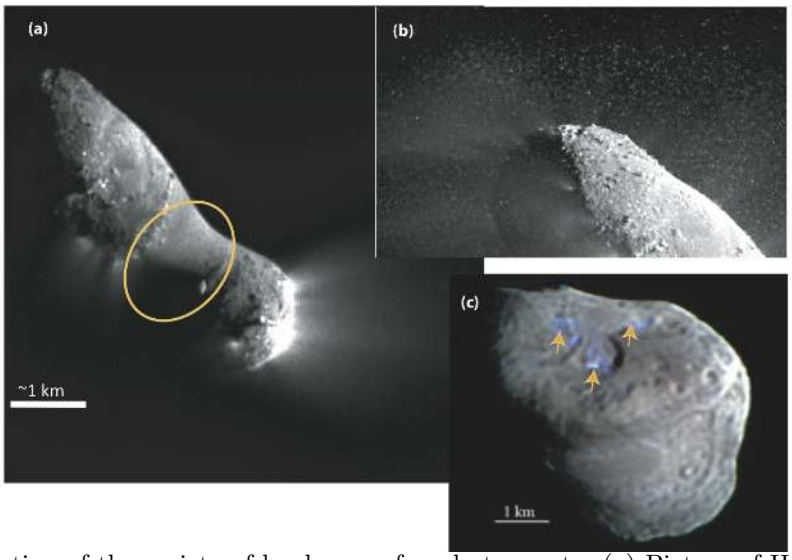

Figure 10: Illustration of the variety of landscapes found at comets. (a) Picture of Hartley 2 obtained by EPOXI showing a contrast in surface roughness between active and waste areas. (b) This close up shows the variations of physical properties, especially roughness, at all scales. (c) In this close-up picture of Tempel 1 observed by Deep Impact lateral variations in chemistry (ice and dust) occur on short spatial scales.

Objectives	Observations	Measurements	Architecture
Distinguish signature of accretion environment from evolution processes, identify sampling sites	Quantify diversity and relationship between units	High resolution imaging and spectral mapping, fine chemical properties (APXS, Raman, UV, XRD)	Mapping from orbiter followed by sampling at multiple selected areas
Identify genetic relationship with other volatile-rich bodies	Volatile and isotopic composition	High resolution imaging (WAC+NAC), gravity	Reconnaissance of water-rich areas by orbiter followed by in-situ measurements
Understand the processes driving cometary activity	Study venting area and relationship with the environment	UV imaging, high-res imaging	Orbital identification of venting features followed by in-situ measurements of dynamic events by multiple redundant surface assets (in order to decrease risk)
Characterize astrobiological significance	Characterize environment, search for hydrothermal signature	Raman/LIBS, APXS, mid-IR, XRF/XRD	In situ measurements at multiple locations since orbital reconnaissance is difficult

Table 3: Cometary science and relevant instruments and architectures.

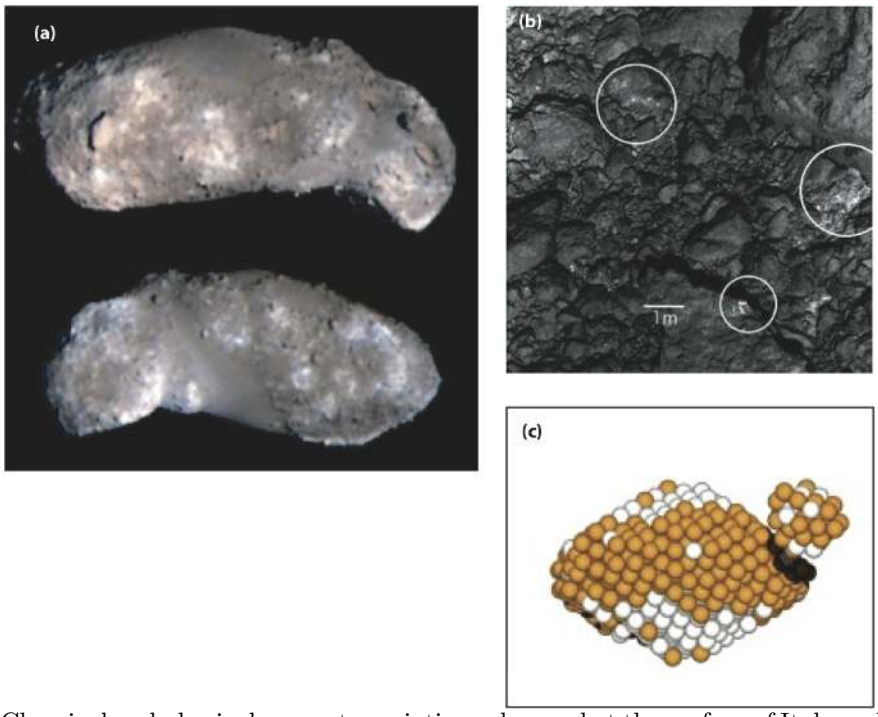

Figure 11: (a) Chemical and physical property variations observed at the surface of Itokawa by the *Hayabusa* mission. The surface shows significant lateral variations in roughness determined in large part by the gravity field. Local surface overturn (due to landslides or impacts) has exposed "fresh" material whose high albedo significantly contrasts with the overall dark color of the asteroid's weathered surface. (b) High-resolution view of the surface illustrating the hazardous conditions presented to human exploration. (c) Result of the simulation of binary asteroid formation [26] as a consequence of high-velocity spinning of the original parent body; spinning results in the redistribution of material from the equator to the poles and the exposure of pristine material (orange) buried below the regolith layer (white).

Objectives	Observations	Measurements	Architecture
Determine surface mechanical properties	Soil competence, granularity at all scales, gravity	High resolution imaging, gradiometer, mechanical tester	Reconnaissance with orbiter, track rover's motion and interaction with dust
Search for in-situ resources	Chemical and mineralogical composition	NIR, GRaND, APXS	Remote sensing from orbiter, in-situ characterization at selected sites
Characterize risk and search for mitigation approaches	Waves and fields (e.g., electrostatic field), dust dynamics	UV imaging, high-res imaging	In situ
Understand and simulate human activities in low-gravity environment	Simulate digging, sampling	Performance	In situ

Table 4: Near Earth Objects.

3 Spacecraft/rover hybrid: mobility concept

A spacecraft/rover hybrid is a small (≈ 0.4 m geometrical diameter, ≈ 5 kg even though the design is scalable) multi-faceted geometric solid that encloses three mutually orthogonal flywheels and is surrounded by external spikes or specialized contact surfaces (see Figure 12, where we consider a cube geometry; design considerations are discussed in detail in Section 3.3). Specifically, there is no external propulsion. The combination of the flywheels with the enclosure- and spike-geometry enables controlled tumbles, hops, and high-altitude ballistic flight.

The basic principle behind a flywheel is the conservation of angular momentum, which ensures that angular momentum can be swapped between the platform and the flywheels. Specifically, a flywheel consists of a spinning mass with a substantial amount of inertia. Due to the presence of the flywheels, the total angular momentum of the platform is given by (vectors and matrices are represented in boldface):

$$\mathbf{H} = \mathbf{I}_{\text{platform}}\,\boldsymbol{\omega}_{\text{platform}} + \sum_{i=1}^{3} \mathbf{I}_{\text{flywheel},i}\,\boldsymbol{\omega}_{\text{flywheel},i},$$

where $\mathbf{I}$ denotes the inertia matrix and $\boldsymbol{\omega}$ denotes the angular velocity vector. Since, in absence of *external* torques, the total angular momentum stays constant, by controlling the *internal* torque between the flywheels and the platform one can control both magnitude and direction of the angular rotation of the platform. In turn, this angular rotation can give rise to (controllable) surface reaction forces at contact points, which lead to either tumbling (i.e., pivoting around a tip) or hopping (when the reaction forces are large enough). The next section presents a 2D analytical model (amenable to analytical treatment) where collisions with ground are assumed inelastic and impulsive, and a 3D model (studied numerically) where contact interactions are modeled according to a spring-damper combination.

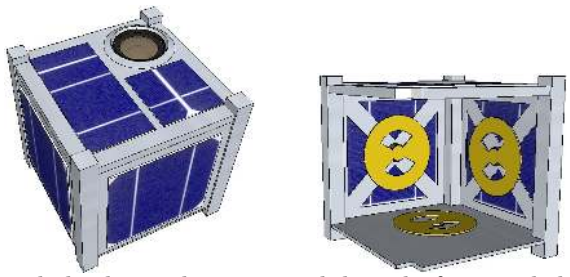

Figure 12: A spacecraft/rover hybrid is a planetary mobility platform sealed in one enclosure and actuated through three mutually orthogonal flywheels (for clarity, internal payload is not shown). By spinning the flywheels, one gives rise to surface reaction forces that make the rover tumble or hop. External spikes/feet (not shown here for clarity) are added to protect instruments and solar panels, and to improve traction. Trade-offs for spike design are discussed in Section 3.3.

3.1 Dynamics of a hybrid

In this section we present both a 2D and a 3D model for a hybrid.

3.1.1 2D analytical model

In the analytical model, the hybrid is modeled in 2D as a disk with equispaced rigid spikes attached to it; a motor, attached at its center of mass, drives a single disk-shaped flywheel

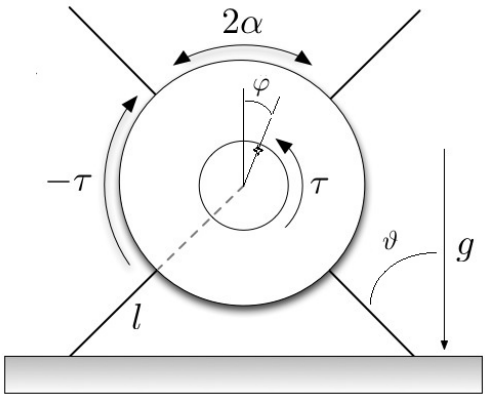

	Definition
ϑ	hybrid's angle
φ	flywheel's angle
m_{rw}	mass of platform
m_{fw}	mass of flywheel
l	spikes' length
r_{rw}	radius of platform
r_{fw}	radius of flywheel
τ	flywheel's torque
2α	angle in between spikes
g	gravity acceleration

Figure 13: Analytical model; collisions with ground are inelastic and impulsive.

(see Figure 13). We use a disk shape since this leads to slightly simpler formulas; the results we obtain, however, represent a reasonable approximation for other symmetrical geometries (e.g., squares) with the same geometrical diameter. The key assumptions in this model are: (1) collisions with ground are inelastic and impulsive (only angular momentum is conserved around the point of collision, and the spike sticks to the ground); (2) the stance foot acts as a pin joint and does not slip, and (3) the transfer of support at the time of contact is instantaneous (no double support phase). This model is inspired by work in the field of passive dynamic walking [28, 29] and, specifically, is based on the model in [30]. With this model we aim to characterize the 2D tumbling motion, in particular, required torques, momentum unloading strategies, and bounds on achievable speeds in microgravity. Even though the assumptions of this model are somewhat unrealistic (especially on small bodies), the results we obtain provide valuable first-order estimates for the aforementioned quantities (as also confirmed by experiments reported in Section 3.4).

Tumbling motion The 2D flywheel-driven hybrid has two states, namely the angle ϑ between the stance spike and the vertical and the angle φ of a reference point on the flywheel with respect to the vertical (see Figure 13); note that we use the convention that angles increase in the clockwise direction. The parameters of the system are defined in Figure 13.

The goal of the control strategy for the flywheel is to cause the platform to tumble to the right, stepping from spike to spike. A complete step is composed of a *stride* phase and a *collision* phase [30]. The stride phase occurs when the system is supported by a single spike. The collision phase occurs when the next consecutive spike collides with the ground. We first consider the stride phase. The equations of motion are those of an inverted pendulum and can be written as

$$\ddot{\vartheta}(t) = \frac{(m_{\text{rw}} + m_{\text{fw}}) g\, l \sin(\vartheta(t)) - I_{\text{fw}} \ddot{\varphi}(t)}{(m_{\text{rw}} + m_{\text{fw}}) l^2 + I_{\text{rw}}}. \tag{1}$$

In our model we assume that the motor is a conventional DC motor and that, as is typical, there is a fast inner feedback loop to control the current. Hence, the armature current is our control input. Since the armature current is linked to the flywheel's acceleration (assuming negligible friction) through a scale factor, henceforth we will consider as *equivalent* input the

flywheel's acceleration.

Second, we consider the equations of motion during the collision phase. The angular momentum (about the contact point) of the system evolves according to the equation: $\mathbf{L}(t) = \mathbf{L}(t_0) + \int_{t_0}^{t} \mathbf{T}_{\text{ext}}(t)\, dt$, where $\mathbf{T}_{\text{ext}}(t)$ represents the external torques acting on the system. During impact the only external torque is due to gravity (all other torques are internal and cancel each other), and is given by $\mathbf{T}_{\text{ext}}(t) = (m_{\text{rw}} + m_{\text{fw}}) g\, l \sin(\vartheta(t))(-\mathbf{e}_z)$ (where $\mathbf{e}_z$ is the unit normal vector outward from the plane). Since $\|\mathbf{T}_{\text{ext}}(t)\| \leq (m_{\text{rw}} + m_{\text{fw}}) g\, l \sin(\alpha)$ and since the collision with the ground is impulsive (i.e., the collision time dt approaches zero), during a collision the angular momentum is (approximately) conserved. The conservation of angular momentum during collision allows for the determination of the initial state for the next stride phase. Specifically, the angular momentum about the collision point of next spike immediately before collision is $\mathbf{L}(t^-) = (m_{\text{rw}} + m_{\text{fw}})\dot{\vartheta}(t^-) l^2 \cos(2\alpha)(-\mathbf{e}_z) + I_{\text{rw}}\dot{\vartheta}(t^-)(-\mathbf{e}_z) + I_{\text{fw}}\dot{\varphi}(t^-)(-\mathbf{e}_z)$, while the angular momentum about the collision point of next spike immediately after collision is $\mathbf{L}(t^+) = (m_{\text{rw}} + m_{\text{fw}})\dot{\vartheta}(t^+) l^2 (-\mathbf{e}_z) + I_{\text{rw}}\dot{\vartheta}(t^+)(-\mathbf{e}_z) + I_{\text{fw}}\dot{\varphi}(t^+)(-\mathbf{e}_z)$. Assuming that $\ddot{\varphi}(t)$ is a bounded function (as it is true for any physical system), one has $\dot{\varphi}(t^-) = \dot{\varphi}(t^+)$, and therefore equating the magnitudes of $\mathbf{L}(t^-)$ and $\mathbf{L}(t^+)$ one obtains:

$$\dot{\vartheta}(t^+) = \frac{(m_{\text{rw}} + m_{\text{fw}}) l \, \cos(2\alpha) + I_{\text{rw}}}{(m_{\text{rw}} + m_{\text{fw}}) l + I_{\text{rw}}} \, \dot{\vartheta}(t^-). \tag{2}$$

Hence, the angular velocity for the next stride phase is reduced (by a factor $\cos(2\alpha)$ if I_{rw} is negligible), as it is expected since collisions are assumed inelastic. As in [28, 30], we define η as the loss coefficient for the angular speed, i.e.,

$$\eta := \frac{\dot{\vartheta}(t^+)}{\dot{\vartheta}(t^-)} = \frac{(m_{\text{rw}} + m_{\text{fw}}) l \, \cos(2\alpha) + I_{\text{rw}}}{(m_{\text{rw}} + m_{\text{fw}}) l + I_{\text{rw}}}.$$

We consider next three cases of increasing complexity, namely: unactuated flywheel, constant actuation, and time-varying actuation. When the flywheel is unactuated (i.e., $\ddot{\varphi}(t)$ is identically zero during the stride), the minimum initial angular speed to vault the hybrid over the stance spike and take a step is:

$$\omega_{\min} := \sqrt{\frac{2(m_{\text{rw}} + m_{\text{fw}}) g\, l (1 - \cos(\alpha))}{(m_{\text{rw}} + m_{\text{fw}}) l^2 + I_{\text{rw}}}}.$$

According to the loss equation (2), an unactuated hybrid will asymptotically come to rest. The aim of the flywheel controller is then to regain, during the stride phase, the speed lost during the impact.

The simplest possible actuation for the flywheel is to have a constant acceleration during the stride phase (i.e., $\ddot{\varphi}(t) = \ddot{\overline{\varphi}} < 0$, negative because it is opposite to tumbling direction). Assume that the angular speed at the beginning of a stride phase is $\dot{\vartheta}(0) := \omega_{\text{ini}} \geq \omega_{\min}$; by using energy arguments, one can easily show that the required acceleration to maintain the same angular speed at the beginning of each subsequent stride phase is:

$$\ddot{\overline{\varphi}} = -\dot{\vartheta}^2(0) \, \frac{\frac{1}{2}\big[(m_{\text{rw}} + m_{\text{fw}}) l^2 + I_{\text{rw}}\big](1/\eta^2 - 1)}{2\alpha I_{\text{fw}}}, \tag{3}$$

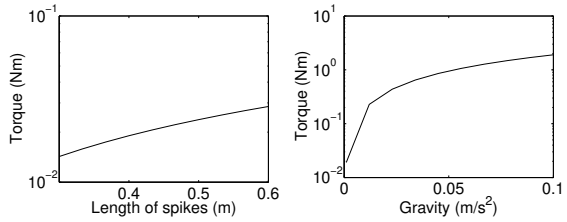

(a) Torques for *tumbling* motion. Left figure: torque vs. spikes' length (gravity $g = 0.001$ m/s^2). Right figure: torque vs. gravity (spikes' length $l = 0.4$ m).

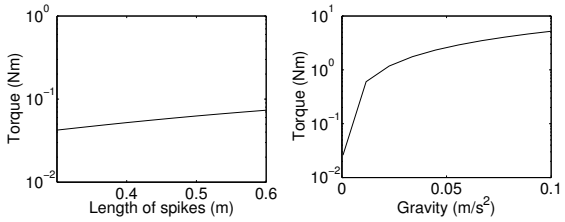

(b) Torques for *hopping* motion. Left figure: torque vs. spikes' length (gravity $g = 0.001$ m/s^2). Right figure: torque vs. gravity (spikes' length $l = 0.4$ m).

Figure 14: Minimum torques for tumbling and hopping motion (the y-axis is in logarithmic scale). System's parameters: platform's mass equal to 2.9 kg, flywheel's mass equal to 0.1 kg (hence the total mass is 3 kg), radius of platform equal to 0.2 m, and 4 spikes (hence $\alpha = \pi/4$). Longer spikes facilitate tumbling over large rocks but require higher torques.

which depends on gravity since we assumed $\dot{\vartheta}(0) \geq \omega_{\min}$. Figure 14(a) shows the magnitude of the minimum torques for a Phobos-like environment (i.e. g in the 0.001 m/s^2 range). Assuming that the flywheel is powered by a "conventional" DC motor, one can conclude that for a gravity level similar to the one on Phobos the power consumption is about $2-5$ Watts. The corresponding linear velocity for tumbling is about 0.05 m/s (Phobos's escape velocity is about 11 m/s). Clearly, this control strategy is not physically realizable since the flywheel will eventually reach a *saturation* speed. It is of interest to characterize the number of strides the flywheel can operate before it saturates. To first order terms, the duration of a stride is given by $\tau_{\text{stride}} = 2\,\alpha/\dot{\vartheta}(0)$. Hence, if $\dot{\varphi}_{\max}$ is the maximum angular speed of the flywheel, the system can operate for a number of cycles (i.e., strides) equal to:

$$N_{\max} = \frac{2\,\dot{\varphi}_{\max}\, I_{\text{fw}}}{\dot{\vartheta}(0)[(m_{\text{rw}} + m_{\text{fw}})l^2 + I_{\text{rw}}](1/\eta^2 - 1)}.$$

For a Phobos-like environment (i.e. g in the 0.001 m/s^2 range), assuming that the maximum rpm for the flywheel motor is 10,000, the maximum number of cycles is then equal to $\simeq 160$ (or about 150 m). A few comments are in order. First, one can see that with realistic values for the system parameters (e.g., the gravity acceleration is similar to that of Phobos) the platform can tumble at an average speed of 3 cm/s for about 150 m drawing a current of about 0.002 A. Second, the formula for the constant acceleration control (equation (3)) shows that such value depends quadratically on the length of the spikes, hence there is an important tradeoff between the capability of negotiating obstacles (that would require long spikes) and the amount of actuation (that prefers short spikes). Third, the actuation level depends quadratically on the desired angular speed. Fourth, as already mentioned, the above control strategy has the disadvantage that after some time the flywheel will reach the saturation limit for its speed. This issue will be addressed in more detail at then end of this section.

Finally, by allowing a time-varying actuation for the flywheel, one can guarantee, perhaps surprisingly, that the angular speed of both the platform *and* the flywheel are the same at the beginning of each stride (i.e., there is forward motion but no net increase in flywheel's

speed). Following [30], this can be achieved through a 4-step control strategy: 1) while ϑ is negative the flywheel is negatively accelerated ($\ddot{\varphi} < 0$); 2) when ϑ becomes positive the flywheel is positively accelerated (i.e., $\ddot{\varphi} > 0$) in such a way that the rotation of the system is stopped (i.e., $\dot{\vartheta} = 0$) and for a certain interval of time (depending on η) angular momentum is accumulated; 3) the flywheel is negatively accelerated to quickly reduce its speed to the initial speed; 4) the flywheel is then left unactuated until collision (i.e., until $\vartheta = \alpha$).

It is of interest to characterize the fundamental limitations of performance for control policies that avoid a build-up in flywheel's velocity. By rather simple angular momentum arguments (see [30, page 24] for the details of a very similar derivation), one can show that a hybrid undergoing a steady-state (i.e., with equal angular velocity at each start of stride) tumbling motion with zero initial and final flywheel speeds and with non-negative net flywheel rotation can travel at a ground speed no larger than:

$$v_{\max} := \frac{2l \sin(\alpha) \, (m_{\rm rw} + m_{\rm fw}) \, g \, l \, \sin(\alpha)}{\sqrt{2\alpha \, (1-\eta)[(m_{\rm rw} + m_{\rm fw})l^2 + I_{\rm rw}]}}.$$

For a Phobos-like environment and hybrid's parameters as in Figure 14, $v_{\max} \approx 5\,\text{cm/s}$.

Hopping A very similar analysis can be performed for the hopping motion. Specifically, we studied the following model: a hybrid starts by rotating around a spike according to the tumbling motion described in the previous section. When the next spike impacts the ground, we still assume that the collision is impulsive and inelastic and that the transfer of support is instantaneous; however, we do not constrain the new stance foot to act as a pin joint, and we study the minimum angular speed that makes the hybrid "hop" or, more precisely, makes the stance foot complete a rotation of 2α without contacting the ground. One can show that hopping is achieved with a constant flywheel deceleration (assuming no saturation) equal to:

$$\ddot{\overline{\varphi}} \leq -\frac{g}{I_{\rm fw}} \min\Big\{ (m_{\rm rw}+m_{\rm fw})l \, \sin(\alpha), \frac{(m_{\rm rw}+m_{\rm fw})l^2+I_{\rm rw}}{4\,\eta^2\, l \, \cos(\alpha)\, \alpha} \Big\}.$$

Figure 14(b) shows the magnitude of the minimum torques for a Phobos-like environment.

Desaturation strategies for the flywheel A key feasibility aspect for such mobility concept is flywheel's speed saturation. The simple 2D model suggests several strategies to mitigate this problem. The first and second strategies were previously discussed: operate without consideration of saturation; and careful acceleration and deceleration of the flywheel such that forward motion is produced without a net increase in flywheel speed. The first strategy is reasonable for very low gravity and/or moderate coverage requirements ($\approx 100\,\text{m}$ for Phobos-like conditions). The second is most effective, but requires sophisticated sensing and control. Third strategy: after a certain number of tumbles/hops, the flywheel is slowly despun in such a way that the platform does not tip over. This strategy is simple but substantially decreases the hybrid's average speed. Fourth strategy (in some sense dual of the third strategy): the flywheel is slowly accelerated (such that the platform does not tip over) and then decelerated in a very short time interval (by using brakes). In this way the hybrid starts a hop/tumble with a flywheel angular velocity of zero. This strategy is further developed in Section 3.2.

3.1.2 3D numerical model

Prior work on microgravity mobility has either simulated dynamics of rigid bodies without motion planning [8, 31], or studied planning algorithms for mobility platforms modeled as point masses [32]. Here we present a 3D model for the hybrids that will be used in Section 3.2 to develop planning algorithms on a realistic, rigid body representation of the hybrid. This model allows for the elimination of some of the assumptions required for the analytical model (e.g., single contact point acting as a pivot). By extending the work in [33], the Newtonian equations for the equations of motion for the hybrid (including the internal flywheels) are as follows (the notation is defined in Table 5):

- Position and velocity:

$$
\begin{aligned}
{}^{\mathrm{b}}\dot{\mathbf{r}}_{\mathrm{cm}} &= {}^{\mathrm{b}}\mathbf{v}_{\mathrm{cm}}, \\
{}^{\mathrm{b}}\dot{\mathbf{v}}_{\mathrm{cm}} &= \frac{\mathbf{F}}{m_{\mathrm{tot}}} - 2\left({}^{\mathrm{I}}\boldsymbol{\Omega}_{\mathrm{bd}} \times {}^{\mathrm{b}}\mathbf{v}_{\mathrm{cm}}\right) - \left({}^{\mathrm{I}}\alpha_{\mathrm{bd}} \times {}^{\mathrm{b}}\mathbf{r}_{\mathrm{cm}}\right) - \\
&\qquad {}^{\mathrm{I}}\boldsymbol{\Omega}_{\mathrm{bd}} \times \left({}^{\mathrm{I}}\boldsymbol{\Omega}_{\mathrm{bd}} \times {}^{\mathrm{b}}\mathbf{v}_{\mathrm{cm}}\right).
\end{aligned}
$$

- Euler parameters:

$$
\begin{bmatrix} {}^{\mathrm{b}}\dot{\epsilon}_1 \\ {}^{\mathrm{b}}\dot{\epsilon}_2 \\ {}^{\mathrm{b}}\dot{\epsilon}_3 \\ {}^{\mathrm{b}}\dot{\epsilon}_4 \end{bmatrix} = \frac{1}{2} \begin{bmatrix} {}^{\mathrm{b}}\epsilon_4 & -{}^{\mathrm{b}}\epsilon_3 & {}^{\mathrm{b}}\epsilon_2 & {}^{\mathrm{b}}\epsilon_1 \\ {}^{\mathrm{b}}\epsilon_3 & {}^{\mathrm{b}}\epsilon_4 & -{}^{\mathrm{b}}\epsilon_1 & {}^{\mathrm{b}}\epsilon_2 \\ -{}^{\mathrm{b}}\epsilon_2 & {}^{\mathrm{b}}\epsilon_1 & {}^{\mathrm{b}}\epsilon_4 & {}^{\mathrm{b}}\epsilon_3 \\ -{}^{\mathrm{b}}\epsilon_1 & -{}^{\mathrm{b}}\epsilon_2 & -{}^{\mathrm{b}}\epsilon_3 & {}^{\mathrm{b}}\epsilon_4 \end{bmatrix} \begin{bmatrix} {}^{\mathrm{b}}\omega_1 \\ {}^{\mathrm{b}}\omega_2 \\ {}^{\mathrm{b}}\omega_3 \\ 0 \end{bmatrix}.
$$

- Angular velocities:

$$
\begin{bmatrix}
I_1 & 0 & 0 & J_{\mathrm{B}}\beta_{\mathrm{B}_1} & J_{\mathrm{C}}\beta_{\mathrm{C}_1} & J_{\mathrm{D}}\beta_{\mathrm{D}_1} \\
0 & I_2 & 0 & J_{\mathrm{B}}\beta_{\mathrm{B}_2} & J_{\mathrm{C}}\beta_{\mathrm{C}_2} & J_{\mathrm{D}}\beta_{\mathrm{D}_2} \\
0 & 0 & I_3 & J_{\mathrm{B}}\beta_{\mathrm{B}_3} & J_{\mathrm{C}}\beta_{\mathrm{C}_3} & J_{\mathrm{D}}\beta_{\mathrm{D}_3} \\
\beta_{\mathrm{B}_1} & \beta_{\mathrm{B}_2} & \beta_{\mathrm{B}_3} & 1 & 0 & 0 \\
\beta_{\mathrm{C}_1} & \beta_{\mathrm{C}_2} & \beta_{\mathrm{C}_3} & 0 & 1 & 0 \\
\beta_{\mathrm{D}_1} & \beta_{\mathrm{D}_2} & \beta_{\mathrm{D}_3} & 0 & 0 & 1
\end{bmatrix}
\begin{bmatrix}
{}^{\mathrm{I}}\dot{\omega}_1 \\ {}^{\mathrm{I}}\dot{\omega}_2 \\ {}^{\mathrm{I}}\dot{\omega}_3 \\ {}^{\mathrm{s}}\dot{\omega}_{\mathrm{B}} \\ {}^{\mathrm{s}}\dot{\omega}_{\mathrm{C}} \\ {}^{\mathrm{s}}\dot{\omega}_{\mathrm{D}}
\end{bmatrix} =
$$

$$
\begin{bmatrix}
M_1 + (I_2 - I_3)\,{}^{\mathrm{I}}\dot{\omega}_2\,{}^{\mathrm{I}}\dot{\omega}_3 + \sum_{\mathrm{k}\,=\,\mathrm{B,C,D}} \left(J_{\mathrm{k}}\,{}^{\mathrm{s}}\omega_{\mathrm{k}} \left(\beta_{\mathrm{k}_2}\,{}^{\mathrm{I}}\omega_3 - \beta_{\mathrm{k}_3}\,{}^{\mathrm{I}}\omega_2\right)\right) \\
M_2 + (I_3 - I_1)\,{}^{\mathrm{I}}\dot{\omega}_3\,{}^{\mathrm{I}}\dot{\omega}_1 + \sum_{\mathrm{k}\,=\,\mathrm{B,C,D}} \left(J_{\mathrm{k}}\,{}^{\mathrm{s}}\omega_{\mathrm{k}} \left(\beta_{\mathrm{k}_3}\,{}^{\mathrm{I}}\omega_1 - \beta_{\mathrm{k}_1}\,{}^{\mathrm{I}}\omega_3\right)\right) \\
M_3 + (I_1 - I_2)\,{}^{\mathrm{I}}\dot{\omega}_1\,{}^{\mathrm{I}}\dot{\omega}_2 + \sum_{\mathrm{k}\,=\,\mathrm{B,C,D}} \left(J_{\mathrm{k}}\,{}^{\mathrm{s}}\omega_{\mathrm{k}} \left(\beta_{\mathrm{k}_1}\,{}^{\mathrm{I}}\omega_2 - \beta_{\mathrm{k}_2}\,{}^{\mathrm{I}}\omega_1\right)\right) \\
\dfrac{{}^{\mathrm{s}}\mathbf{M}_{\mathrm{B}} \cdot \vec{\beta_{\mathrm{B}}}}{J_{\mathrm{B}}} \\
\dfrac{{}^{\mathrm{s}}\mathbf{M}_{\mathrm{C}} \cdot \vec{\beta_{\mathrm{C}}}}{J_{\mathrm{C}}} \\
\dfrac{{}^{\mathrm{s}}\mathbf{M}_{\mathrm{D}} \cdot \vec{\beta_{\mathrm{D}}}}{J_{\mathrm{D}}}
\end{bmatrix}.
$$

The external loads, $\mathbf{F}$, and external moments, $\mathbf{M}$, are calculated according to a simple spring-damper-friction contact model. The force normal to the ground is modeled as a spring-damper system and transverse forces are calculated using a Coulomb friction model. While these models are reasonably accurate for hard surfaces, soft, granular media (as it is

	Definition
${}^{\mathrm{b}}\mathbf{r}_{\mathrm{cm}}$	position of spacecraft cm w.r.t. celestial body
${}^{\mathrm{b}}\mathbf{v}_{\mathrm{cm}}$	velocity of spacecraft cm w.r.t. celestial body
$\mathbf{F}$	net external force on spacecraft
m_{tot}	total mass of spacecraft w/ flywheels
${}^{\mathrm{I}}\mathbf{\Omega}_{\mathrm{bd}}$	angular velocity of celestial body w.r.t. inertial
${}^{\mathrm{I}}\alpha_{\mathrm{bd}}$	angular acceleration of celestial body w.r.t. inertial
${}^{\mathrm{b}}\epsilon_{\mathrm{i}}$	i^{th} Euler orientation parameter w.r.t. celestial body
${}^{\mathrm{b}}\omega_{\mathrm{i}}$	i^{th} angular velocity of craft w.r.t. celestial body
${}^{\mathrm{I}}\omega_{\mathrm{i}}$	i^{th} angular velocity of craft w.r.t. inertial
I_i	i^{th} principle MOI of craft about cm
J_{k}	axial MOI of flywheel k (k = B, C, D)
$\vec{\beta}_{\mathrm{k}}$	axis of rotation of flywheel k w.r.t. spacecraft
${}^{\mathrm{s}}\omega_{\mathrm{k}}$	angular velocity of flywheel k w.r.t. spacecraft
${}^{\mathrm{s}}\mathbf{M}_{\mathrm{k}}$	torque on flywheel k from spacecraft
M_k	i^{th} component of net external torque on spacecraft

Table 5: Notation for the dynamics equations.

the case for regoliths) requires a more sophisticated contact model, which is left for future work.

In the above dynamics equations, except for the terms ${}^{\mathrm{s}}\mathbf{M}_{\mathrm{k}} \cdot \vec{\beta}_{\mathrm{k}}$, all of the variables are either state variables, or contact forces that are found by solving the set of differential equations, or terms that are known a priori. Each ${}^{\mathrm{s}}\mathbf{M}_{\mathrm{k}} \cdot \vec{\beta}_{\mathrm{k}}$ term represents the torque applied along the central axis of the kth flywheel and acts as one of the control inputs to the system. A predetermined profile of the control variables must be fed into the system (open-loop control), or closed-loop control must be used to generate these values during the simulation. Section 3.2 details a closed-loop, hybrid approach for the flywheels to achieve waypoint tracking.

3.2 Planning and control

The current computational model is restricted to uniform gravity fields and perfectly spherical terrains. Even under these idealized conditions, motion planning and control is still a significant challenge. The main difficulties stem from the gyroscopic coupling of the rotational degrees of freedom due to flywheel motion, and the unpredictable nature of hopping/bouncing due to the hybrid's non-spherical shape.

Our approach consists of a simple 3-mode hybrid control algorithm, whereby the flywheels are slowly accelerated to a desired angular velocity (referred to as "objective net angular velocity"), and then impulsively braked to generate the torque needed to produce hopping/tumbling. Figure 15 diagrams the control modes and the switching conditions.

Specifically, the key idea behind the proposed motion planning algorithm is that the net angular velocities of the flywheels prior to braking should form a vector that is mutually orthogonal to both the heading and local gravity vectors. In this way, the torque from braking the flywheels causes the hybrid to tumble or hop in the general direction of the next waypoint. Deviations from the intended hopping direction, caused by a non-spherical geometry (e.g. edges, spikes), are compensated for by applying this approach to a sequence

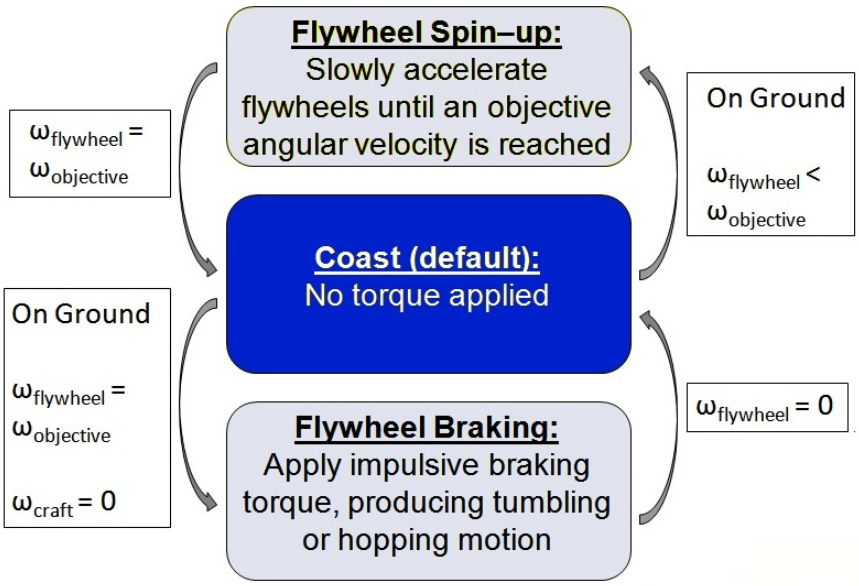

Figure 15: Hybrid control algorithm: controlled mobility is achieved by slowly accelerating and then impulsively braking the flywheels. The angular velocity to which each flywheel is accelerated is determined by the hybrid orientation and intended heading. Additional control is used to ensure unwanted tumbling does not occur during the Spin-up mode.

of hops/tumbles. Accordingly, the direction of the objective net flywheel angular velocity prior to braking is

$$\hat{\omega}_{\text{objective}} = \frac{\vec{h} \times \vec{g}}{\left|\vec{h} \times \vec{g}\right|}, \tag{4}$$

where $\hat{\omega}_{\text{objective}}$ is the unit vector of the objective net angular velocity of flywheels, $\vec{g}$ is the local gravity vector, and $\vec{h}$ is the heading vector to the next waypoint (see Figure 16). The *magnitude* Ω of the objective net angular velocity of the flywheels is calculated according to two rather natural guidelines: (1) the hybrid attempts to travel from its current location to the next waypoint via an ideal hop (45° launch vector), and (2) the rotational kinetic energy stored in the flywheels before braking is approximated as equal to the translational kinetic energy of the hybrid after braking. A brief comment on these guidelines: they are fundamentally approximations (i.e. the hybrid does *not* travel to each waypoint via a single hop and the two energy terms are not exactly equal), however their enforcement leads to a simple, yet effective computation of the control inputs. Specifically, let v_0 be the velocity of the hybrid just after braking; according to guideline (1), $v_0^2 = gh$, where h is the distance to be traveled. Applying guideline (2), we obtain:

$$\underbrace{\frac{1}{2} k_p m_{tot} v_0^2}_{\text{translational}} = \underbrace{\sum \frac{1}{2} I_k \omega_k^2}_{\text{rotational}},$$

where ω_k is the angular velocity of the kth flywheel prior to braking, m_{tot} is the total mass of the hybrid ($m_{\text{rw}} + \sum m_{\text{fw},k}$), and the control gain k_p is used to account for energy losses.

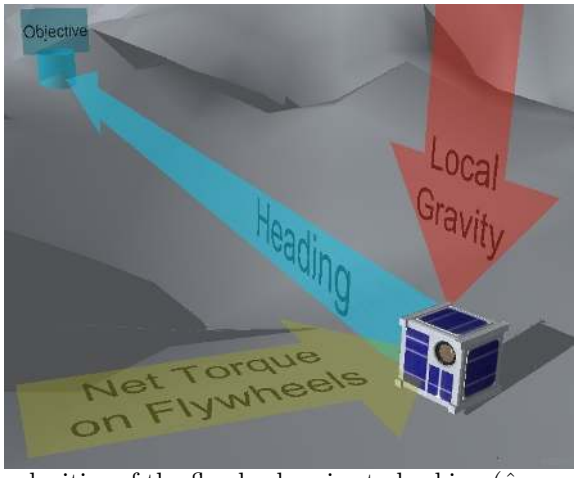

Figure 16: The net angular velocities of the flywheels prior to braking ($\hat{\omega}_{\text{objective}}$) should form a vector that is roughly anti-parallel to the net torque on the flywheels during braking (yellow arrow in above figure). This set of vectors is defined to be mutually orthogonal to both the heading and local gravity vectors according to equation (4).

Since, by definition, $\omega_k = \Omega\, \hat{\omega}_{\text{objective}} \cdot \vec{\zeta}_k$, where $\vec{\zeta}_k$ is the unit vector of the kth flywheel's central axis, one can readily solve for Ω as

$$\Omega = \sqrt{\frac{k_p m_{tot}\, gh}{\sum I_k \left(\hat{\omega}_{\text{objective}} \cdot \vec{\zeta}_k\right)^2}}.$$

The objective angular velocity for each flywheel is then:

$$\omega_k = \left(\sqrt{\frac{k_p m_{tot}\, gh}{\sum I_k \left(\hat{\omega}_{\text{objective}} \cdot \vec{\zeta}_k\right)^2}}\right) \hat{\omega}_{\text{objective}} \cdot \vec{\zeta}_k. \tag{5}$$

Once the objective angular velocities are determined (by using equations (4) and (5)), the flywheels are slowly accelerated to these velocities so as to ensure that unwanted tumbling (i.e. tumbling away from the next waypoint) does not occur. The analytical model of the hybrid (see Section 3.1) is used to estimate the maximum torque that does not induce tumbling. Feedback control is then used to ensure that tumbling does not occur during the flywheel spin-up. Once the objective angular velocities are reached, brakes are applied to the flywheels to induce hopping motion. An upper bound is put on the flywheel velocities to model flywheel saturation and a lower bound is imposed on the objective angular velocity to ensure that some motion occurs for each spin-and-brake sequence. No control is applied while the hybrid is in ballistic flight or while it is coming to a rest. This process is repeated until the hybrid comes to rest within a tolerance region of each waypoint. Successful execution of this algorithm for four arbitrary waypoints is displayed and discussed in Figure 17. Our simulation results assume a smooth surface; future work should address the case of rocky terrains and non-uniform gravity levels.

3.3 Prototype and design considerations

A first generation of spacecraft/rover hybrids was developed to validate the results of the computer simulations. The prototype and CAD models for the structure and the flywheels

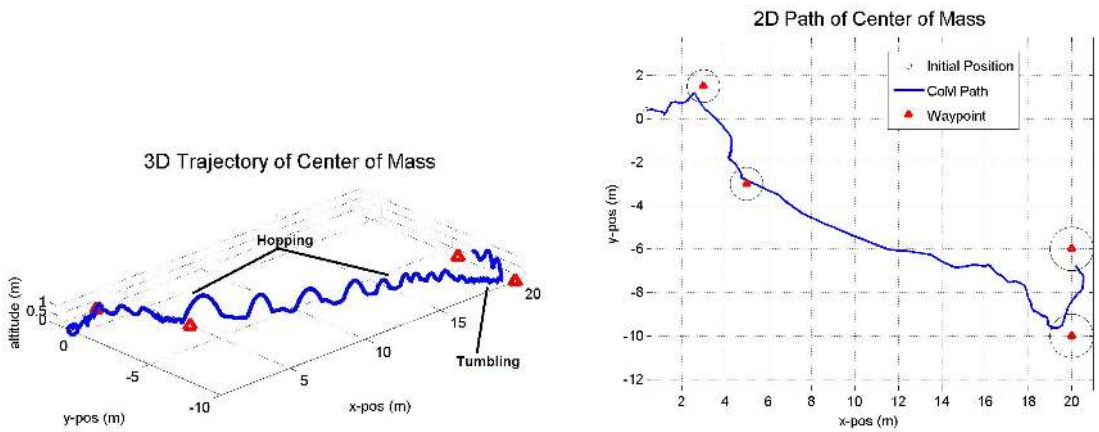

Figure 17: Demonstration of *controlled* mobility (as opposed to random hopping motion): the plots represent the application of the motion planning and control algorithm under Phobos-like conditions (i.e., gravity levels on the order of $\mathrm{mm/s^2}$). Waypoints were selected to demonstrate short and long traverses and directional changes. The hybrid averages a velocity of $\approx 1.6\,\mathrm{cm/s}$ over the 1770 seconds it takes to visit the four waypoints. This velocity compares well with the analytical results from Section 3.1 which established a maximum achievable tumbling velocity of $\approx 5\mathrm{cm/s}$.

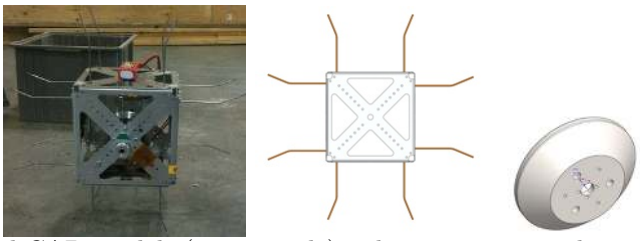

Figure 18: Prototype and CAD models (not to scale). The prototype, without the flywheel, has a mass of 1.39 kg and a moment of inertia about the axis of rotation of $\approx 0.054\,\mathrm{kg\,m^2}$. The flywheel is 0.57 kg and $8.07 \times 10^{-4}\,\mathrm{kg\,m^2}$.

are given in Figure 18. The design includes one internal motor/flywheel combination aligned with the unconstrained rotational degree of freedom on the passive gravity off-load test stand we developed (this test stand consists of a gravity off-load system of pulleys and a counterweight; more details about this test stand are provided in Section 3.4). The test vehicle also includes an Arduino microcontroller to coordinate motion and capture data, an 11.9V DC battery for power, and an electronic speed controller. An optical rpm sensor measures and records flywheel speeds, and the torques applied during experimentation are calculated as $\tau_{\mathrm{applied}} = I_{\mathrm{fw}}\alpha_{\mathrm{fw}}$.

The motor/flywheel subsystem consists of a brushless DC motor capable of spinning the flywheel at up to 12,000 rpm. All components in the system were designed with that maximum speed in mind. The flywheel was designed to be as close as possible to the center of the vehicle without interfering with the proposed additional flywheels in the full 3-axis vehicle. The result is a tapered flywheel that balances minimization of the system's moment of inertia and mass with maximization of the flywheel's moment of inertia.

The overall structure and frame of the system consists of a cube with a 20 cm edge and with 4 spikes per face. The spikes include a bend to create a regular octagon with 20 cm on each side. Additional mass was added to balance the vehicle around the rotation axis as well as across the vehicle left to right. No attempt was made to balance the weight around the

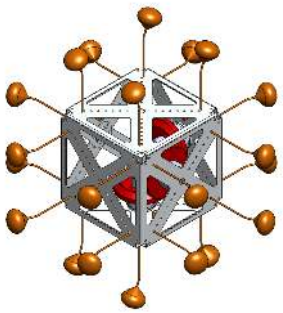

Figure 19: Second prototype of the hybrid. Note the lilypad design of the tips of the spikes.

vertical z-axis on this initial prototype. The design and the geometry of the spikes require a special discussion. Computational studies showed that distributing the contact forces over the maximum area (i.e. direct contact between the vehicle's enclosure and terrain; no spikes) make for the most robust mobility in varying terrain conditions (e.g. soft regolith, hard rocks), see [31]. On the other hand, spikes are needed to form a stand-off distance so that solar panels and instruments are protected from unintended impacts with hard rock fragments, and to negotiate large obstacles. As a compromise, spikes should be employed with properly designed feet to increase contact area and avoid sinkage in loose terrain. This design compromise is represented in the second prototype of the hybrid that uses spikes with lilypad-like tips (see Figure 19). Next section discusses experimental results from two different 3 Degree of Freedom (DOF) test stands.

3.4 Experimental results

Due to the difficulty of emulating milli- to microgravity conditions, many testing approaches were considered. Two testing methods, counter-weighted pendulum and frictionless table, satisfied time and budget constraints. These methods, and corresponding experimental results, are discussed in more details below. Other methods that were considered, yet not feasible for the timeframe or budget of this research included parabolic flights, drop towers, actively controlled gantry crane, robotic arms, balloon-assisted offload, and buoyancy tanks.

3.4.1 Experiments on counter-weighted pendulum

We performed experiments on a low-gravity 3 DOF test stand to further characterize the dynamics of the hybrids and to assess the validity of the models presented in Section 3.1. The test stand consists of a gravity off-load system with pulleys and a counterweight. Two off-load cables are used to prevent rotation about the vertical axis due to gyroscopic precession. This test stand introduces pendulum dynamics that quickly dominate all motion, yet it can still provide valuable information about the initial conditions of a hop or tumble. The effective gravity is determined both statically, with a high precision scale, as well as dynamically by collecting data while dropping the test vehicle on the stand and measuring its vertical acceleration. Two configurations were used, a 2 m test stand and a 5 m test stand. Experiments were run by programming a pre-defined acceleration (therefore torque) profile into the Arduino microcontroller (that runs the flywheel's DC motor). The experimental torque profiles were then used in the 3D simulation environment to control a model of the prototype. The goal of these tests was to compare the torque levels at which hopping/tumbling are ini-

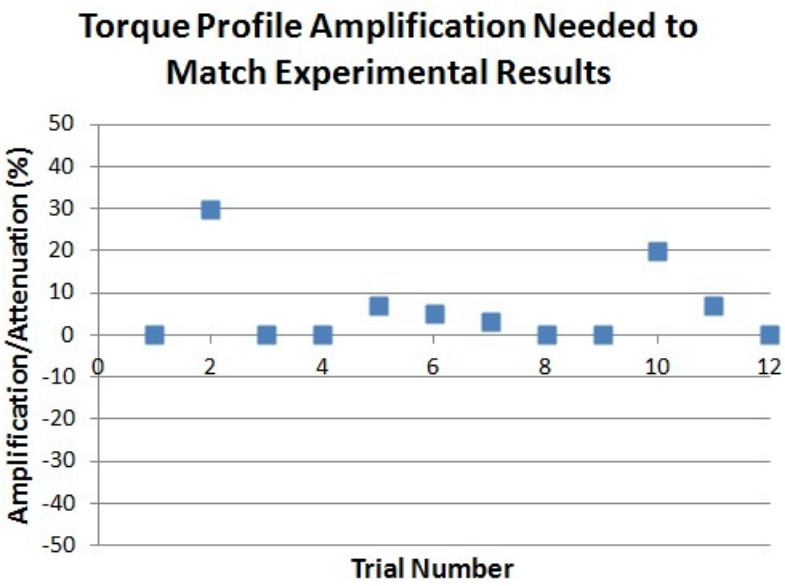

Figure 20: Experiment-simulation comparison: values indicate the amount by which the torque profile had to be modified in simulation to match motion observed in experiments. The effective gravity for this set of experiments was 0.235 m/s^2 .

tiated both during the experiments and in simulation (some disagreement is expected due to modeling approximations and the pendulum dynamics introduced by the pulley mechanism of the test stand). Specifically, if behaviors did not match (e.g. experiment demonstrated tumbling but the simulation did not), then the torque profile would be amplified or attenuated until similar behavior was observed. Figure 20 summarizes the results from the experiment-simulation comparisons. The key result is that an average torque amplification of only 6% is required for the simulation to emulate the experiments.

3.4.2 Experiments on frictionless table

We also developed a 3 DOF test stand that relies on a frictionless table and does not require any pulley system (and, hence, does not introduce any exogenous dynamics). The test stand consists of a metallic plate that is air-bearing supported over a table and of a flywheel attached at the top. The table is slightly tilted in order to emulate a low-gravity environment in 2D (with an emulated gravity of about 0.05 m/s^2), see Figure 21. Baking flour is used as a simulant for regolith found in microgravity environments. We recorded tumbling speeds of $\approx$ 2 cm/s and hops up to distances of $\approx$ 0.5 m (longer hops were theoretically possible, but could not be implemented due to the size of the granite table). In general, experimental results on this test stand were in agreement with the results from the pulley system test stand, the analytical models, and the numerical simulations.

3.5 Summary

The cross-validation of analytical, simulation, and experimental results shows that a hybrid, with a limited amount of power, can achieve both tumbling and hopping motion with velocities on the order of several cm/s (depending on gravity) and with a motion accuracy on the order of 10%; furthermore, several mitigation strategies are possible to deal with flywheel saturation. These results were obtained, however, under the assumption of a smooth terrain

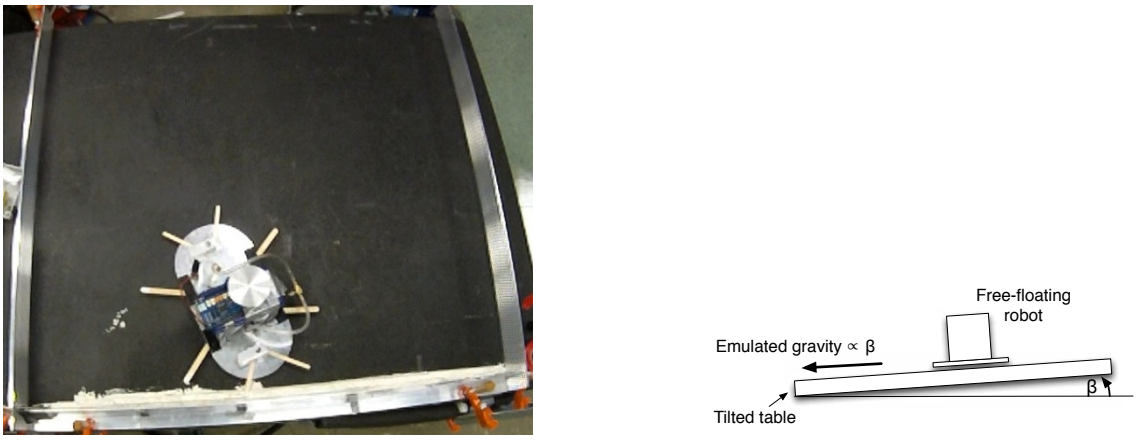

Figure 21: 3 DOF test stand on a frictionless table; by tilting the granite table, one can create a "small" force that emulates a low gravity field.

on a non-rotating body with uniform gravity. Deployment on a relevant environment has to face two main challenges. The first set of challenges is related to the presence of rocks and boulders, which make the bounces rather unpredictable; this makes the selection of the initial hopping direction and attitude control during ballistic flight pivotal to ensure motion accuracies in the 20-30% range. Furthermore, some regions might be covered with loose dust and the hybrids could sink and become "stuck". Assuming that such regions can be detected, it becomes paramount to be able to plan trajectories *around* or *over* them. Rocks would also complicate the task of instrument pointing. The second set of challenges is related to the geometrical and dynamical properties of the target body. On a rotating body, the motion of a robotic platform can be significantly influenced by the Coriolis and centripetal accelerations, which can make potential regions of interest (e.g., those around an unstable equilibrium for motion dynamics) hard to reach [34].

4 Spacecraft/rover hybrid: subsystems

In this section we provide first-order estimates for critical subsystems of the hybrids, including power supply, communication, thermal, and localization.

4.1 Power supply

As discussed before, each actuator would draw about $2 - 5$ Watts. In Phase I we also estimated a power consumption of ≈ 3 Watts for the onboard computer, of ≈ 8 Watts for communication, and of ≈ 5 Watts for scientific instruments. According to the operational modes that we identified (see Section 5), the average power consumption for a Phobos-like environment is on the order of 15 Watts. In Phase I we have studied in detail the simplest possible strategy, which involves the usage of primary batteries, with no recharging capability. The conclusion is that the lifetime of the hybrid would be limited to a couple of days at most. As is discussed in Section 5, operating the hybrids will involve completely new procedures and will surely involve an extended learning curve. This makes the lifetime limitation imposed by using primary batteries inadvisable, unless several hybrids are deployed sequentially or there is already some legacy for their operations. To increase hybrids' lifetime beyond 48 hours, one could consider a combination of solar panels and secondary batteries. Solar panels would be placed on the exterior of the hybrid, in the spaces between the spikes. The critical concerns for this system would be the available area for solar cells and the possibility of the cells being covered with dust from the regolith. Given that only the tips of the spikes will make contact with the surface, and there are no thrusters to stir up dust, the solar cell/secondary battery choice may represent an acceptable risk. However, given the uncertainty of the dust environment, it may be that (miniaturized) RTGs would provide a less risky power alternative, despite the cost and regulatory issues; recent breakthroughs in this field might make this option viable. Another option would be advanced regenerative fuel cell systems.

4.2 Thermal control

Thermal requirements will differ depending on the environment being explored. We have carried out a preliminary thermal analysis for a hybrid resting on the sub-Mars point in Stickney crater on Phobos, i.e., at the equator, assuming 15 Watts of power generated inside the hybrid. Phobos's rapid movement (7.66 hour orbit) helps average out the hot and cold parts of the orbit. Our first-order estimates show a thermal time constant on the order of the orbital period, with an average temperature slightly above freezing. Hence, at least for Phobos, passive thermal protection, with coatings and multi-layer insulation, could be acceptable.

4.3 Shielding against electrostatic effects

We determined that if the electrostatic field is less than 100 V (as appears typical for small bodies), electrostatic charging should not represent a significant problem for hybrids' operations (especially telecom). Indeed, since the hybrid would be continuously tumbling, its overall charge should rapidly reach an equilibrium with the surface. The only phase that could represent a risk is the night-day transition; a possible solution would be to turn off all telecom and have a first period during which the hybrid "shakes" itself by tumbling.

4.4 Communication

We have considered various communications schemes for the hybrid. We have assessed that it is not practical for the hybrid to carry a directional antenna for direct communication with Earth. Therefore, the hybrid would use the mothership as a relay both for data and commands. We have considered various antenna schemes for the hybrid and identified the opportunity to take advantage of the hybrid's spikes by using two opposing spikes as the elements of a dipole antenna. Specifically, the current design involves two opposing spikes of the hybrid as the elements of a dipole antenna. Because the hybrid may come to rest in arbitrary orientations, one needs to ensure against having the mothership ending up in the direction of a low node in the dipole antenna pattern. A possibility would be to use three orthogonal pairs of spikes to create three orthogonal dipoles. Sensors, either on the mothership or on the hybrid, could measure RF signal strength and route all power to the most favorable dipole. Another possibility would be to use of polarization sensing by the mothership as a tool for determining the hybrid's azimuthal orientation. Any antenna on the mothership capable of high data rate communication with Earth will be able to communicate with a several watt dipole on the hybrid. Using the same antenna for Earth and hybrid communications would, however, require periodic reorientation of the mothership attitude and would significantly increase the time required to get data from the hybrid to the Earth and to get commands to the hybrid.

4.5 Localization

In the Phase I study, we have considered both dynamic sensors (such as accelerometers, gyros, and contact sensors) and vision sensors (i.e. cameras on the hybrid). Through dynamic sensors the hybrids can reconstruct their trajectory and hence determine their current position; however, this approach leads to large position errors due to sensors' drifts. This motivates the usage of vision sensors, which are able to provide "absolute" position measurements. However, the small and compact shape of the hybrids severely constrains the baseline for stereo vision (hence precluding precise depth estimation), a significant percentage of images would be captured from a low vantage point, and the continuously rotating field of view would make the estimation process particularly challenging and computationally expensive. The conclusion is that, given the low mass, low volume, and the limited computation capabilities of the hybrids, one should consider *synergistic mission operations*, wherein the mothership bears the primary responsibility for determining the position and orientation of the hybrid, and the mobile platform is only responsible for local perception. Within this architecture, localization of the hybrids would be done through a combination of sensors onboard the mothership and sensors onboard the hybrid. The hybrids would carry only a minimal suite of navigational sensors to keep the complexity, computation and power of the hybrid to a minimum. The navigational sensors would include a MEMS inertial measurement unit, one or more wide-angle cameras (e.g., to detect the *local* environment, such as the presence of nearby rocks and craters), a means to sense contact on the spikes, and possibly one or more sun-sensors (for rough attitude determination). The major hurdle associated with this architecture is its sensitivity to reliable telecommunication.

4.6 On board handling and telemetry

Because of the discontinuous communication contacts with the mothership, each hybrid would need to operate autonomously, collecting, compressing, and storing data until each uplink opportunity. In cases of low radiation environment, an FPGA, small micro-controller or micro-processor solution would be strong candidates with relatively high density memory. The nature of the scientific payload would naturally allow for a high degree of sequential operation with initial uplink of accelerometer data, followed by in-situ data. Given the general simplicity of the hybrid compared to most other interplanetary spacecraft, we do not anticipate the computer system posing any particular difficulties.

4.7 Summary

The Phase I study has determined that most subsystems could be implemented with existing technologies. On the other hand, given the low-mass, small-scale of a hybrid, localization should rely on novel synergistic mission operations, whereby the localization and guidance systems would be split in between the hybrid itself and the mothership. This would require a substantial technology development. Also, a future effort should explore life-expanding power subsystem approaches including a combination of solar panels and secondary batteries, and low-cost, miniaturized Radioisotope Thermoelectric Generator (RTG) technologies currently under development.

5 Mission architecture

5.1 Four-phase mission operation

In the Phase I study we have performed a preliminary study for mission operations, *under the assumption that the mothership is already in proximity of the target body*. We have then specialized our study to a mission to Phobos. At a high-level, the plan for mission operations involves four main phases:

1) Initial reconnaissance of object: The operational objective of this mission phase is to select an area on the object where the hybrid can initially be placed.

2) Deployment of hybrid: The mothership releases the hybrid so as to place it on the surface of the object as near as possible to the selected site. There are two possible scenarios: in-situ deployment with a touch-and-go maneuver or deployment from a distance. While the first scenario is arguably the safest for the hybrids, it involves significant risks (e.g., JAXA's Hayabusa failed this maneuver [10]) and requires sophisticated guidance for the mothership, which translates into a high-cost dedicated mission. In the second scenario, there are three significant risks: the hybrid might crash on the surface, might bounce off the object and become "lost in space", or might penetrate deep enough into the surface so as to become "stuck". We have studied this scenario in detail for a reference mission to Phobos and determined that 3 m/s is approximately the touchdown speed from the Halo orbit at Mars-Phobos L1 (while this may seem fast, note that is the equivalent of dropping an object from a height of ≈ 50 cm on the Earth), with a settling time on the order of a few hours. Hence, for the proposed mission to Phobos (discussed below), release from a distance could be a feasible option. In general, release from a distance is the preferable option, provided that *safe* deployment strategies can be developed.

3) Initial "free roaming": The hybrid is commanded to perform several episodes of unguided motion, with increasing durations. The unguided motions are analyzed back on Earth to determine how well the hybrid's behavior compares to preflight simulations.

4) Command and execute guided trajectories: Since the hybrid will be visible to the mothership only during daylight and some measurements would benefit from the low-noise night environment, the hybrid would move during the day and would acquire measurements during the night. One of the most critical problems is surface operations for the hybrids. After a trade-off study (see also the previous discussion about localization), the Phase I has determined that: a) autonomous operations for the hybrids would require a robotic platform that is a spacecraft in its own right (hence, no longer minimalistic), b) similar performance can be obtained at a potentially reduced cost through synergistic mission operations, where the hybrid relies on the mothership for localization and for part of the trajectory planning process. This assumes, however, a reliable, high-bandwidth telecommunication channel. Next section discuss in more details guidance, navigation, and control within a synergistic mission operations scenario.

5.2 Guidance and navigation with synergistic mission operations

In a synergistic approach, the Navigation, Guidance, and Control functions are embedded within the mothership as follows.

Navigation: The goal is to determine the position of the hybrid on the surface of the body and to ascertain its orientation. As far as *orientation* is concerned, sensitive accelerometers

would enable the hybrid to determine on its own its orientation with respect to the local vertical. The more difficult task is to determine its azimuthal orientation about the local vertical. This is a function where the mothership would have to play a critical role. The most obvious technique is optical. This requires a camera on the mothership obtaining a high-resolution image of the hybrid resting on the surface, a larger-scale context image of the surface, and some markings on the hybrid that would allow optical correlation of the orientation of the hybrid with respect to the surface. Differentiating azimuthal segments of the hybrid to allow optical identification would be a challenge, made more difficult by potential dust contamination. Perhaps blinking lights could provide a solution. Another technique would be for the mothership to measure the direction of linear polarization from one of the hybrid's dipole antennas, from which it could determine the hybrid's azimuthal orientation. Finally, the mothership could command a motion about a specific hybrid body axis. The mothership would visually record the actual motion, from which Mission Control could figure out how the hybrid had been oriented.

Determining the *position* of the hybrids would make use of sensors both on the hybrid and the mothership. A feature-based temporal matching technique, known as visual odometry, has been used for estimating the pose on Mars rovers [35]. While, as discussed before, such techniques cannot be readily applied to the hybrids, the idea of matching visual features to estimate pose can be *adapted* to this unique platform (indeed, some preliminary work to adapt visual odometry to hopping platforms is already available [36, 37, 38]). In our case, using onboard stereo imaging would likely not fit within the envisioned mass and volume of the hybrids. However, a less accurate approach that relies on *monocular* vision would be sufficient for the hybrids. Since the hybrid's onboard computation would be limited, the hybrid can be restricted to executing canned sequences that acquire the necessary information and send it to the mothership. To generate three-dimensional information, one can envision the hybrid acquiring an image in the direction of travel and then slowly tumbling in the lateral direction counting contacts with the ground to establish an approximate baseline. The two images and approximate baseline would be uploaded to the mother craft to process the data. The mother craft would identify tie-point features between two or more temporal frames separated by the approximate baseline(s) to establish a camera model. Using this model, it would compute a low-resolution dense three-dimensional map, on which the position of the hybrid can be located. Future work should develop the algorithms to implement such strategy, and should perform a validation on a hardware testbed.

Guidance & Control: Narrow field-of-view imaging sensors on the mothership operating at several kilometers from the small body surface would provide contextual images for operating the hybrids. These images would be used in conjunction with hybrids' navigation data to perform the motion planning process discussed in Section 3.

5.3 Reference mission to Phobos

In the Phase I study we performed a preliminary mission analysis for a Phobos mission scenario; the results in this section significantly leverage the work in [39], concurrently performed by one of the Co-Is. In summary, a single-string electric propulsion mothership would deploy from a distance one, or more, hybrids on the surface of Phobos in proximity of the Stickney crater (see Figure 22). Such platforms would carry a X-ray spectrometer, a radiation monitor, a thermocouple, and a microscope, and would operate for about 48

hours over a surface of about $1-5\,\mathrm{Km}^2$. The mothership would be equipped with a gamma ray and neutron detector, a high-resolution stereo camera, a radio science subsystem, and a dust analyzer, and would station keep at the Mars-Phobos L1 point, see Figure 22. Using orbital observations, mission planners would upload traverse sequences to the hybrids via the mothership (see Figure 23). Major science objectives would be to characterize regolith composition, evaluate regolith maturity, constrain mechanical properties, constrain dust dynamics, achieve both topography and gravity mapping, study surface dynamics and the electrostatic environment, and characterize the distribution of water. In the next sections we give more details about the different parts of the mission.

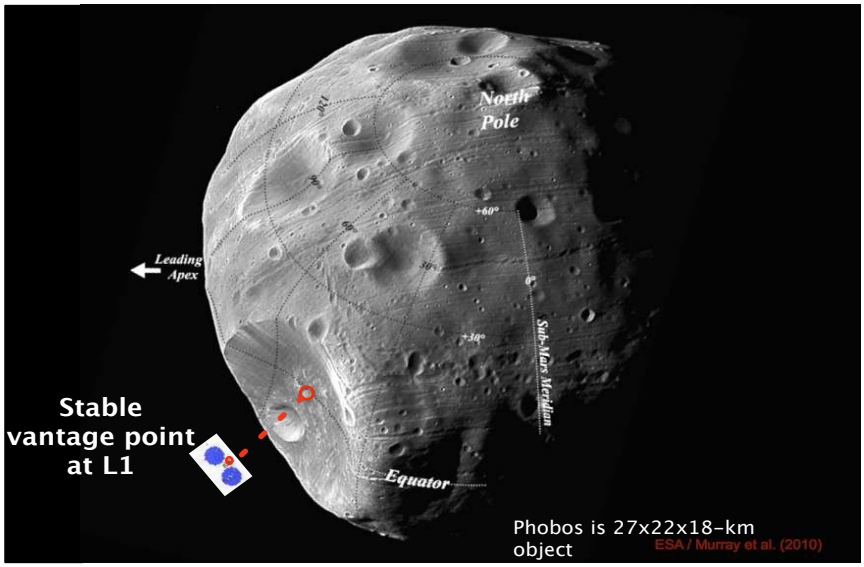

Figure 22: Mission architecture: the mothership (Phobos Surveyor, see Figure 24) would deploy on the surface of Phobos one or more hybrids and would station keep at the Mars-Phobos L1 point.

5.3.1 Science objectives and hybrid's design

Our high-level mission study led to the science traceability matrix presented in Table 6 (that considers miniaturized instruments with TRL 6 or higher) and to a desired path for the hybrid that is represented in Figure 23 and is aimed at sampling both physical and chemical diversity. Certain measurements are best achieved by the mothership (e.g., global reconnaissance, gravity, topography) while others can be performed only in-situ (e.g., soil properties). In other words, the mothership would provide broad area coverage, while the hybrid would zoom in on specific areas and conducts in-situ measurements. Hence, the responsibility for primary science would be shared between the mothership and the hybrid. The science objectives shown in Table 6 would be achieved with a hybrid having a motion accuracy of 20%-30%, which compares well with the capabilities of a hybrid.

Table 7 shows the baseline design for the hybrid; the total mass would be about 5 kg and the average power requirement would be approximately equal to 15 Watts.

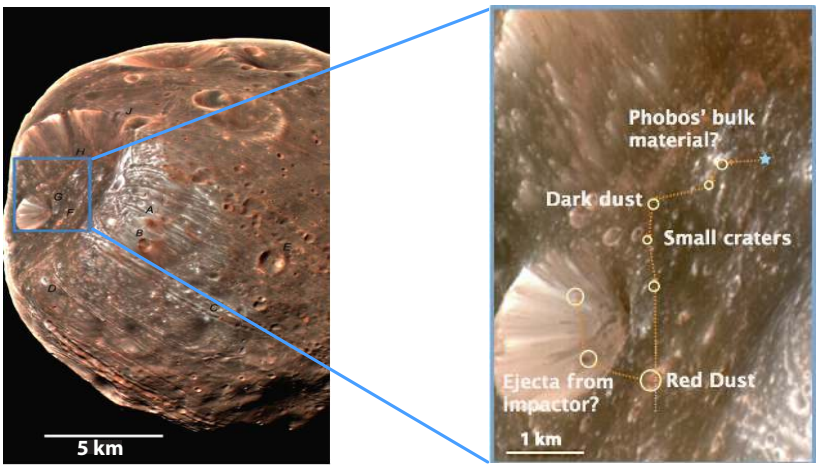

Figure 23: Notional illustration of the trajectory that a hybrid should execute in order to sample both the chemical and the physical diversity on Phobos (close to the Stickney crater). The motion accuracy, given the scale of the landmarks to be visited, should be on the order of $20\% - 30\%$, which compares well with the capabilities of a hybrid.

Theme	Objectives	Observable	Role	Instrument
Decadal: Origins **Precursor: Soil mechanics/risk**	Obtain regolith composition	Elemental	Mothership	GR&ND
		Mineralogical	**Hybrid**	XRS
	Evaluate regolith maturity	Microstructure	**Hybrid**	Microscope
	Constrain mechanical properties	Angle of repose	**Hybrid**	Camera
		Response to impulse	**Hybrid**	Accelerometers
		Crater morphology	Mothership	HRSC
	Constrain dust dynamics	Measure dust flux	Mothership	Dust analyzer
Decadal: Processes **Precursor: Risk**	Topography mapping	Photoclinometry	Mothership	HRSC
	Gravity mapping	Doppler tracking	Mothership	RSS
		Acceleration	**Hybrid**	Accelerometers
	Assess surface dynamics & electrostatic environment	Dust interaction with spikes	**Hybrid**	Camera
Decadal: Habitability **Precursor: ISRU**	Distribution of water	Neutron detection	Mothership	GR&ND
		Mineralogical	**Hybrid**	XRS

Table 6: Traceability matrix for a reference mission to Phobos (XRS = X-ray spectrometer, GR&ND = Gamma Ray and Neutron Detector, HRSC = High-Resolution Stereo Camera, RSS = Radio Science Subsystem). "Decadal" stands for science highlighted in the decadal survey, while "Precursor" stands for science in support of precursor missions. The mothership payload is tailored to provide information on the geological and geophysical *context*, while the in-situ element is meant to acquire observations of the soil properties with the resolution necessary to address the goals of origins and precursor science.

	Instrument	Mass (g)	Power (Watts)
Science Package	Radiation monitor	30	0.1
	XRS	300	4
	Thermocouple	50	1
	Microscope	300	0.1
Operational and science support	Accelerometer/Tiltmeter	66	0.002
	Descent camera (WAC/PanCAM)	100	0.1
Subsystems	Transceiver	230	8
	Avionics (including OBDH)	250	3
	Thermal	200	0
	Antenna	200	0
	Motors and flywheels	400 (total)	3 (each)
Structural	Solar panels	300	
	Battery	222	
	Structure	1000	
	RHU (optional)	400	
		Total $\approx$ 4 kg	**Average**: $\approx$ 12 Watts
		plus 25% margin	plus 25% margin
		Total $\approx$ 5 kg	**Average**: $\approx$ 15 Watts

Table 7: Baseline design for the hybrid for a reference mission to Phobos (WAC = Wide Angle Camera, OBDH= On-Board Data Handling). Total mass would be about 5 kg, and the average power requirement would be about 15 Watts. The enclosure would have, approximately, a 0.25 m radius.

5.3.2 Mothership

The mothership would be the Phobos Surveyor spacecraft (Figure 24), which would provide a low-cost, high reliability approach for a mission to Phobos [39]. Phobos Surveyor can be constructed from currently available, well-characterized commercial components and is capable of carry up to 30 kg of payload into orbit about Mars. Phobos Surveyor would utilize a flight-proven commercial Solar Electric Propulsion (SEP) system; EP systems developed for commercial GEO communication satellites would be perfectly sized for the electrical power and life requirements for a Phobos precursor mission. Two deployable ATK Ultraflex solar arrays would provide sufficient power to operate the EP system at full power while in orbit at Mars. During the Mars Orbit phase (see below), the spacecraft would enter into a 50 min eclipse, relying on a secondary battery to provide power. Due to the low gravity of Phobos, a cold gas RCS thruster could be used to provide enough thruster to safely land the spacecraft (in case of an in-situ deployment of the hybrid). Direct to Earth communication would be achieved using a standard X-band uplink/downlink for science, command and telemetry.

5.3.3 Mission design and operations

Launch and early operations: Mars rideshares provide the most efficient opportunity for the Phobos Surveyor mission, requiring the least transfer propellant. As a SEP mission, the optimal launch time for Phobos Surveyor occurs before the optimal time for a ballistic mission. If unable to utilize a Mars opportunity for rideshare, the Moon becomes the means by which the spacecraft departs to Mars. To leverage the Moon, the mission would require specific targeting allowing for multiple flybys and ultimately Earth departure.

Mars transfer: Figure 25 shows the trajectory from Earth departure to Mars rendezvous. With an Earth departure of 2 km/s, the SEP trajectory does not require thrusting until half way through the transfer, and from that point the trajectory requires constant thrusting to Mars rendezvous.

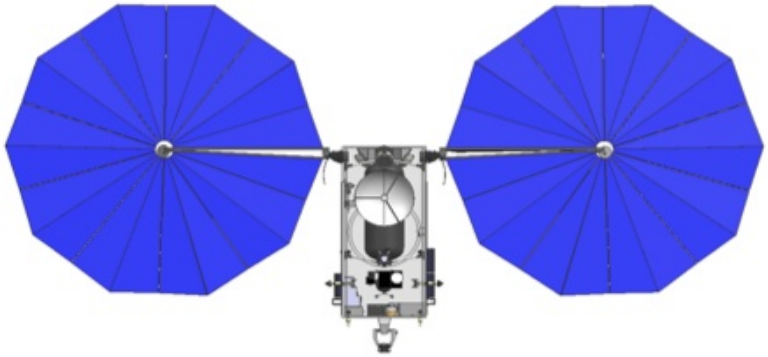

Figure 24: Sketch of Phobos Surveyor. This spacecraft is designed solely out of commercially available off-the-shelf parts [39].

Mars orbit phase The proposed thruster for the Phobos Surveyor mission would be life-limited by propellant throughput. As a result, the spacecraft would be unable to spiral down to Phobos. Consequently, the trajectory would use periapsis thrust arcs, shown in Figure 26, to efficiently reach the Phobos orbit. Within such mission scenario, the transfer time between Mars arrival and Phobos orbit rendezvous would be one year.

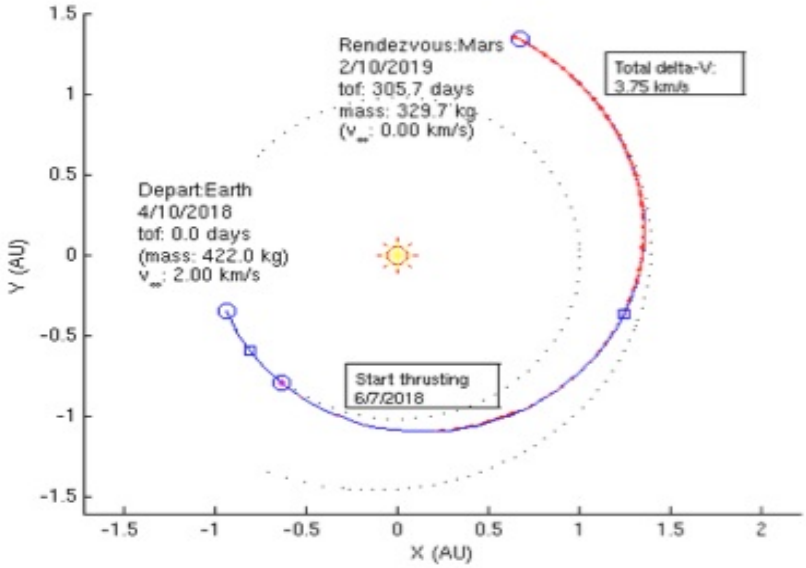

Figure 25: Trajectory from Earth departure to Mars rendezvous [39].

Phobos operations: For close proximity operations, the spacecraft would require autonomous control, similar to JPL's proven AutoNav system used for *DeepImpact*. Requiring more thrust than available from the SEP thruster, the final descent (if needed for the deployment of the hybrid) would utilize the cold gas RCS thrusters. Once the rovers have been delivered, the mothership would remain on a stable station keeping position at the

Lagrangian point above Stickney crater. The GN&C system would utilize a high precision IMU and star tracker measurements to provide attitude feedback to the reaction control system. Torque provided by the reaction wheels would be used to maintain stability and orient the spacecraft for Earth communication.

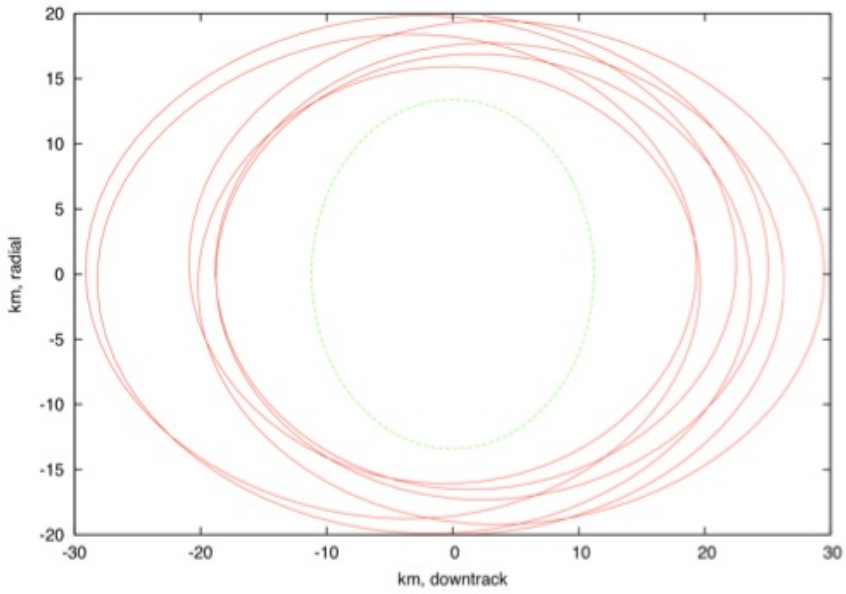

Figure 26: Periapsis thrust arcs to achieve Phobos orbit [39].

5.4 Summary

In summary, the Phase I study has developed a four-phase plan for mission operations. At least for Phobos, release of a hybrid from a distance appears a feasible option. After a trade-off analysis, we determined that, to keep the design of a hybrid as minimalistic as possible, the hybrid should rely on synergistic mission operations, wherein the mothership bears the primary responsibility for determining the position and orientation of the hybrid, and the mobile platform is only responsible for local perception. Two important aspects that remain to be addressed are safe deployment options for the hybrids and detailed definition of synergistic mission operations whereby localization and guidance are split in between the hybrid itself and the mothership.

6 Conclusions

In this effort we investigated a novel mission architecture for the systematic and affordable in-situ exploration of small Solar System bodies. Such a mission architecture stems from a paradigm-shifting approach whereby small bodies' low gravity is directly exploited in the design process, rather than being faced as a constraint. We demonstrated that the bounding assumptions behind our proposed mission architecture are reasonable, with a sound scientific and engineering basis. A future study should focus on the key feasibility and maturation aspects identified during Phase I, in particular, hybrids' fine mobility on irregular terrains, life-expanding power subsystems, and synergistic mission operations.

7 References

[1] Decadal Survey Vision and Voyages for Planetary Science in the Decade 2013–2022. Technical report, National Research Council, 2011. Available at `http://solarsystem.nasa.gov/2013decadal/`.

[2] M. Wargo. Strategic knowledge gaps. 2012. Available at `http://science.nasa.gov/media/medialibrary/2012/05/04/HEOMD_Strategic_Knowledge_Gaps_--_Mike_Wargo.pdf`.

[3] NASA Comet Hopper mission. Technical report, NASA, 2011. Available at `www.lpi.usra.edu/meetings/acm2008/pdf/8131.pdf`.

[4] R.M. Jones. The MUSES–CN rover and asteroid exploration mission. In *22nd International Symposium on Space Technology and Science*, pages 2403–2410, 2000.

[5] M. Chacin, A. Mora, and K. Yoshida. Motion control of multi-limbed robots for asteroid exploration missions. In *Proc. IEEE Conf. on Robotics and Automation*, pages 3037–3042, May 2009.

[6] A. Seeni, B. Schafer, B. Rebele, and N. Tolyarenko. Robot mobility concepts for extraterrestrial surface exploration. In *Aerospace Conference, 2008 IEEE*, pages 1–14, March 2008.

[7] P. Fiorini and J. Burdick. The development of hopping capabilities for small robots. *Autonomous Robots*, 14:239–254, 2003.

[8] C. Dietze, S. Herrmann, F. Kuß, C. Lange, M. Scharringhausen, L. Witte, T. van Zoest, and H Yano. Landing and mobility concept for the small asteroid lander MASCOT on asteroid 1999 JU3. In *61st International Astronautical Congress*, 2010.

[9] R.Z. Sagdeev and A.V Zakharov. Brief history of the Phobos mission. *Nature*, 341:581–585, 1989.

[10] JAXA Hayabusa mission. Technical report, JAXA, 2011. Available at `http://hayabusa.jaxa.jp/e/index.html`.

[11] J. C. Castillo-Rogez, M. Pavone, I.A.D. Nesnas, and J.A. Hoffman. Expected science return of spatially-extended in-situ exploration at small Solar System bodies. In *Aerospace Conference, 2012 IEEE*, pages 1 –15, March 2012.

[12] R. Gomes, H. F. Levison, K. Tsiganis, and A. Morbidelli. Origin of the cataclysmic Late Heavy Bombardment period of the terrestrial planets. *Nature*, 435:466–469, May 2005.

[13] K. Tsiganis, R. Gomes, A. Morbidelli, and H. F. Levison. Origin of the orbital architecture of the giant planets of the Solar System. *Nature*, 435:459–461, May 2005.

[14] A. Morbidelli, H. F. Levison, K. Tsiganis, and R. Gomes. Chaotic capture of Jupiter's Trojan asteroids in the early Solar System. *Nature*, 435:462–465, May 2005.

[15] H. F. Levison, W. F. Bottke, M. Gounelle, A. Morbidelli, D. Nesvorný, and K. Tsiganis. Contamination of the asteroid belt by primordial trans-Neptunian objects. *Nature*, 460:364–366, July 2009.

[16] K.J. Walsh and et al. A low mass for Mars from Jupiter's early gas-driven migration. *Nature*, 475:206–209, September 2011.

[17] H. Campins, K. Hargrove, N. Pinilla-Alonso, E. S. Howell, M. S. Kelley, J. Licandro, T. Mothé-Diniz, Y. Fernández, and J. Ziffer. Water ice and organics on the surface of the asteroid 24 Themis. *Nature*, 464:1320–1321, April 2010.

[18] A. S. Rivkin and J. P. Emery. Detection of ice and organics on an asteroidal surface. *Nature*, 464:1322–1323, April 2010.

[19] Licandro, J., Campins, H., Kelley, M., Hargrove, K., Pinilla-Alonso, N., Cruikshank, D., Rivkin, A. S., and Emery, J. (65) Cybele: detection of small silicate grains, water-ice, and organics. *A&A*, 525:A34, 2011.

[20] Jason C. Cook, Steven J. Desch, Ted L. Roush, Chadwick A. Trujillo, and T. R. Geballe. Near-infrared spectroscopy of charon: Possible evidence for cryovolcanism on kuiper belt objects. *The Astrophysical Journal*, 663(2):1406, 2007.

[21] R. E. Milliken and A. S. Rivkin. Brucite and carbonate assemblages from altered olivine-rich materials on Ceres. *Nature Geoscience*, 2:258–261, April 2009.

[22] Steven J. Desch, Jason C. Cook, T.C. Doggett, and Simon B. Porter. Thermal evolution of Kuiper belt objects, with implications for cryovolcanism. *Icarus*, 202(2):694 – 714, 2009.

[23] B. E. Schmidt and J. C. Castillo-Rogez. Water, heat, bombardment: the evolution and current state of 2 Pallas. *Icarus*, in press, 2012.

[24] B. E. Schmidt and et al. The shape and surface variation of 2 Pallas from the hubble space telescope. *Science*, 326(5950):275–278, 2009.

[25] P. Vernazza, R. P. Binzel, A. Rossi, and M. Fulchignoni. Solar wind as the origin of rapid reddening of asteroid surfaces. *Nature*, 458:993–995, 2009.

[26] K. J. Walsh, D. C. Richardson, and P. Michel. Rotational breakup as the origin of small binary asteroids. *Nature*, 454:188–191, July 2008.

[27] R. Brunetto. Space weathering of small solar system bodies. *Earth, Moon, and Planets*, 105:249–255, 2009.

[28] T. McGeer. Passive dynamic walking. *The International Journal of Robotics Research*, 9(2):62–82, 1990.

[29] K. Byl and R. Tedrake. Metastable walking machines. *The International Journal of Robotics Research*, 28(8):1040–1064, 2009.

[30] G.W. Howell. *Analysis and control of super-articulated biped robots*. Dissertation, Boston University, 2000.

[31] F. Herrmann, S. Kuß, and B. Schäfer. Mobility challenges and possible solutions for low-gravity planetary body exploration. In *ESA/ESTEC*, Noordwijk, Netherlands, April 2011.

[32] Bellerose. J. and D. Scheeres. Dynamics and Control for Surface Exploration of Small Bodies. In *AIAA/AAS Astrodynamics Specialist Conference and Exhibit*, number 6251, Honolulu, HI, August 2008.

[33] T. Kane, P. Likins, and D. Levinson. *Spacecraft Dynamics*, pages 218–223. The Internet-First University Press, 2005.

[34] J. Bellerose, A. Girard, and D. Scheeres. Dynamics and control of surface exploration robots on asteroids. In Michael Hirsch, Clayton Commander, Panos Pardalos, and Robert Murphey, editors, *Optimization and Cooperative Control Strategies*, volume 381 of *Lecture Notes in Control and Information Sciences*, pages 135–150. Springer Berlin / Heidelberg, 2009.

[35] M. Maimone, Y. Cheng, and L. Matthies. Two years of Visual Odometry on the Mars Exploration Rovers. *Journal of Field Robotics*, 24(3):169–186, 2007.

[36] P. Fiorini, C. Cosma, and M. Confente. Localization and sensing for hopping robots. *Autonomous Robots*, 18:185–200, 2005.

[37] E.W.Y. So, T. Yoshimitsu, and T. Kubota. Relative localization of a hopping rover on an asteroid surface using optical flow. In *SICE Annual Conference, 2008*, pages 1727–1732, August 2008.

[38] E.W.Y. So, T. Yoshimitsu, and T. Kubota. Hopping odometry: Motion estimation with selective vision. In *Intelligent Robots and Systems, 2009. IROS 2009. IEEE/RSJ International Conference on*, pages 3808–3813, October 2009.

[39] J. J. Lang, J. D. Baker, J. C. Castillo-Rogez, T. P. McElrath, J. S. Piacentine, and J. S. Snyder. Phobos exploration using two small solar electric propulsion spacecraft. In *Global Space Exploration Conference*, May 2012.